C.P. No. 1267

C.P. No. 1267

PROCUREMENT EXECUTIVE, MINISTRY OF DEFENCE

AERONAUTICAL RESEARCH COUNCIL

CURRENT PAPERS

A Calculation Method for the Two-Dimensional Turbulent Flow over a Slotted Flap

by

H. P. A. H. Irwin

Aerodynamics Dept., R.A.E., Farnborough

LONDON: HER MAJESTY'S STATIONERY OFFICE

1974

PRICE *80p* NET

UDC 532.517.4 : 533.6.011.1 : 533.694.22 :
532.526 : 533.6.048.3 : 532.526.7

CP No.1267 *

June 1972

A CALCULATION METHOD FOR THE TWODIMENSIONAL TURBULENT FLOW OVER A SLOTTED FLAP

by

H. P. A. H. Irwin

SUMMARY

An integral calculation method for the twodimensional turbulent flow over a slotted flap is described, taking into account the interaction of the wake from the main aerofoil with the boundary layer on the flap, and the variation of static pressure normal to the flap surface. The results are compared with experiment, and it is found that the method gives quite good agreement with the measured variation of the integral properties of the wake and boundary layer, and with the measured skin friction. The limitations of the method are discussed briefly in relation to the more complex approach of a differential method.

---

* Replaces RAE Technical Report 72124 - ARC 34236

CONTENTS

1 INTRODUCTION

In the flow over a slotted flap the wake from the main aerofoil and the boundary layer on the upper surface of the flap tend to merge with each other. Some typical total head profiles obtained during experiments described in Ref.1 are shown in Fig.1. From these results it was observed that there is a need for a method of calculating the development of the wake and boundary layer which takes their mutual interaction into account. A particular feature of this flow is the presence of a velocity minimum in the wake and a velocity maximum where the wake meets the boundary layer. With the addition of further auxiliary high lift aerofoils, i.e. slats and vanes, the velocity profile exhibits further maxima and minima, which can disappear as the viscous layer develops downstream. It is likely, therefore, that in the final analysis only a differential calculation method will be sufficiently flexible to deal with all the situations encountered in the flow over aerofoils with high lift devices. At present, however, much remains to be understood of the details of such flows, and so the simplicity of an integral method has advantages in that the empirical assumptions required are usually simpler and can be quickly tested. Also, the accuracy is probably no less than that of a differential method in conditions where the integral method can be applied.

In this Report, therefore, an integral method is described which uses an approach similar to that which Gartshore and Newman[2] applied to the problem of a turbulent walljet in an arbitrary pressure gradient.

2 BASIS OF METHOD

The viscous layer is assumed to consist of three sections: the boundary layer, the inner wake and the outer wake. This enables the velocity profile of the viscous layer to be defined by three mathematical expressions, which in turn require a total of six variables to be defined. The numerical value of each of these six quantities varies in the streamwise direction; integration of the momentum equation for the viscous layer in a direction normal to the stream over five different intervals will yield five of the six equations necessary for the evaluation of these six quantities. The sixth equation is an expression for the rate of change of massflow in the region below the velocity minimum in the wake.

Solution of these six equations requires assumptions to be made regarding the shear stress at five positions in the viscous layer, and also regarding the massflow across the line of minimum velocity. The assumptions made, together with the choice of expressions used for the velocity profiles, are discussed in detail below.

2.1 The velocity profile

In choosing a velocity-profile family simplicity was a primary consideration. The power law is a traditional assumption for boundary layers, and has been used by Gartshore and Newman[2] for walljet calculations. Townsend[3] and Gartshore[4] have used the Gaussian form for wakes, and it was considered that these two forms - power law and Gaussian - could be used both for the condition when the wake and boundary layer are separate (Fig.2a), and when they have merged (Fig.2b).

Using therefore the nomenclature of Fig.2, and considering first the condition where the wake and boundary layer have merged (Fig.2b), the velocity profile of the boundary layer, $0 \leqslant y \leqslant y_{ma}$, is assumed to be

$$\frac{U}{U_{ma}} = \left(\frac{y}{y_{ma}}\right)^{n} \quad . \tag{1}$$

For the inner wake, $y_{ma} \leqslant y \leqslant y_{mi}$, the velocity profile is assumed to be

$$\frac{U}{U_{ma}} = 1 - \frac{(U_{ma} - U_{mi})}{U_{ma}} \exp\left[- k \left(\frac{y - y_{mi}}{L_0}\right)^2 \right] \tag{2}$$

and for the outer wake, $y_{mi} \leqslant y \leqslant \infty$, the velocity profile is assumed to be

$$\frac{U}{U_e} = 1 - \frac{(U_e - U_{mi})}{U_e} \exp\left[- k \left(\frac{y - y_{mi}}{L_1}\right)^2 \right] \quad . \tag{3}$$

The six variables to be determined from the equations are then U_{ma}, U_{mi}, n, y_{mi}, L_0 and L_1.

When the wake and the boundary layer are separated by a region of irrotational flow the velocity profile takes the form shown in Fig.2a. As the 'inviscid' velocity distribution is assumed to be known, the values of the velocity at the inner edge of the wake and at the outer edge of the boundary layer are known, and U_{ma} ceases to be an unknown quantity. It is replaced by L, the width of the irrotational region. However since the Gaussian form, equation (2), would give an infinitely long tail to the inner wake, the inner wake will be truncated at a position $y_{mi} - G_0 L_0$ below the wake centre line. The value of G_0 influences the development of the inner half wake, and also

plays a part in deciding when the region of irrotational flow has disappeared. A value must be found empirically, and the choice of a suitable value is discussed in section 3.3. For similar reasons the outer wake is assumed to end at a position $y_{mi} + G_1 L_1$; the value of G_1 does not have a strong influence on the calculation, and has been chosen such that at $y = y_{mi} + G_1 L_1$ the velocity is given by

$$\frac{U_e - U}{U_e - U_{mi}} = 0.005 \quad .$$

2.2 Integration of the momentum equation

The twodimensional incompressible flow equations for steady flow of a viscous layer along a plane wall are, making the classical assumptions[5],

$$U \frac{\partial U}{\partial x} + V \frac{\partial U}{\partial y} = - \frac{1}{2} \frac{\partial C_p}{\partial x} + \frac{\partial \tau}{\partial y} \tag{4}$$

$$\frac{\partial C_p}{\partial y} = 0 \tag{5}$$

$$\frac{\partial U}{\partial x} + \frac{\partial V}{\partial y} = 0 \quad . \tag{6}$$

Comparison with the exact equations shows that, whilst equation (6) is exact, equations (4) and (5) contain errors of the order of R^{-1}. large R

For flow along a curved wall, of curvature κ, with the co-ordinates x,y measured along the wall and at right angles to it, Goldstein[5] shows that by making similar assumptions to simplify the exact equations as were used for the flow along a plane wall, equations (4) and (6) remain unaltered, whilst equation (5) becomes

$$\frac{\partial C_p}{\partial y} = 2\kappa U^2 \quad . \tag{7}$$

Whilst the term $2\kappa U^2$ is of order $\kappa' R^{-\frac{1}{2}}$, (where $\kappa' = \kappa C$) and, therefore, of higher significance than the terms ignored in the derivation of the equations for the plane wall, the analysis of the flow along a curved wall results in errors of the order of $\kappa' R^{-\frac{1}{2}}$ occurring in the equation for momentum in the x direction (equation 4)) and in the continuity equation (equation (6)) also.

It is not therefore clear *a priori* that the replacement of equation (5) by equation (7) will result in a significant improvement in the overall accuracy of the representation of the motion of the viscous layer.

Nevertheless the experimental results amply demonstrate the existence of a non-zero pressure gradient through the viscous layer, Fig.3. The change of sign of the pressure gradient, as the flow proceeds downstream over the flap, was considered to be due to a change of sign of the curvature of the mainstream flow. This was confirmed by using the method of Hess and Smith[6] to calculate flow velocities both on and near to the flap, under inviscid conditions. Fig.4 shows that the pressure gradient changes sign, even when viscous layers are absent.

In an attempt to ascertain if the pressure gradients result from the curvature of the flow, values of the curvature κ have been derived from Figs.3 and 4, using equation (7) with U assumed to be the local flow velocity. The results of these calculations are given in Table 1. For the first two traverse positions the numerical values agree reasonably well, but this agreement breaks down as the flow approaches the trailing edge of the flap, due to the the rapidly increasing effect of the viscous layer on the real flow, making it markedly different from the inviscid flow. An alternative source of data for the flow curvature was therefore considered, this source being the shapes of the streamlines in the real flow above the flap, shown on Fig.5. By fitting cubic curve to each of the streamlines the variation of curvature along its length could be deduced, and the values obtained in this manner are compared in Table 2 with values of the curvature deduced from the static pressure gradients. Although the agreement is not exact, the values for the downstream stations do show similar trends with distance through the viscous layer.

It would appear, therefore, that the measured static pressure variations do result from the curvature of the flow, and it is very possible that the contribution to the equations of motion from the term involving the static pressure gradient is larger than the contributions given by the similar order terms to the equations involving the x-wise momentum and continuity. The form of the equations given by equations (4), (6) and (7) have therefore been adopted, and upon integrating equation (4) between arbitrary limits y_1 and y_2, and including equation (6), the following equations may be obtained

$$\frac{d}{dx}\int_{y_1}^{y_2} U^2 dy - U_2 \frac{d}{dx}\int_{0}^{y_2} U dy + U_1 \frac{d}{dx}\int_{0}^{y_1} U dy + \frac{1}{2}\int_{y_1}^{y_2} \frac{\partial C_p(y)}{\partial x} dy - (\tau_2 - \tau_1) = 0 \quad \ldots (8)$$

where U_1 and U_2 are the values of U at y_1 and y_2 respectively; τ_1 and τ_2 the corresponding values of τ and $C_p(y)$ the static pressure coefficient at the general point y. The results of substituting the assumed velocity profiles into this equation, and of carrying out the integrations, are given in Appendix A.

2.3 The massflow in the region below the velocity minimum

Analogous with Head's entrainment function[7] a function F is defined as the rate of change of the masflow in the region $0 \leq y \leq y_{mi}$, i.e.

$$F = \frac{d}{dx}\int_{0}^{y_{mi}} U dy \quad (9)$$

F therefore represents the massflow from the outer half wake into the inner half wake. For a wake that is symmetrical both in velocity profile and turbulence structure about its centre, F would be zero. For asymmetric wakes one would intuitively expect the half with the steeper velocity gradient normal to the stream direction to grow at the expense of the other half, and this is borne out by some measurements made during the experiments of Ref.1. In Fig.6 the measured massflow below the velocity minimum is shown for three different flap configurations, and it can be seen that just downstream of the trailing edge of the main aerofoil there was a significant massflow from the outer to the inner half wake, where the steeper velocity gradient normal to the stream existed. Further downstream, as the asymmetry became less, the exchange of mass decreased and, in fact, over a large proportion of the flap chord was almost zero. The experimental point nearest the flap trailing edge, for the case where the flap deflection was 30° and the slot width 0.025c, was almost certainly an overestimate of the massflow, caused by the presence of a sizable region of reverse flow within the boundary layer at that station.

For the purpose of calculating the flow development it appears from Fig.6 that the value of F is sufficiently small over most of the flap for it to be taken as zero. It would be useful, however, if an estimate could be obtained of the effect of non-zero values of F on the calculations and for this purpose a relationship between F and the parameters describing the velocity profile is required. Since little is known about the interaction between the halves of an asymmetric wake there is no readily available expression for F. However, an expression which incorporates the qualitative variation of F observed in the previous paragraph is

$$F = F_s \left(\frac{\left(\frac{\partial U}{\partial y}\right)_{y=y_{mi}-L_0}}{\left(\frac{\partial U}{\partial y}\right)_{y=y_{mi}+L_1}} - 1 \right) \qquad (10)$$

where F_s is a scaling factor. Providing F is small there is some justification for using a relation such as equation (10), despite its crudity, in order to observe the effect of non-zero values of F on the calculations. The scaling factor F_s has been chosen somewhat arbitrarily to be the same as the rate of entrainment of irrotational fluid into the outer half wake, treating it as half of a far wake. Using the entrainment law of Townsend[3] for a far wake the following expression for F_s can then be obtained

$$F_s = 0.31 \frac{U_e \tfrac{1}{2}(U_e - U_{mi})}{U_e + \tfrac{1}{2}(U_e - U_{mi})} \quad . \qquad (11)$$

Substituting for F_s into equation (10) and evaluating the velocity gradients at $y = y_{mi} - L_0$ and $y = y_{mi} + L_1$ the expression for F becomes

$$F = 0.31 \frac{U_e \tfrac{1}{2}(U_e - U_{mi})}{U_e + \tfrac{1}{2}(U_e - U_{mi})} \left[\frac{L_1 (U_{ma} - U_{mi})}{L_0 (U_e - U_{mi})} - 1 \right] \quad . \qquad (12)$$

2.4 The shear stress

The value of the shear stress is required at y equal to zero, $\frac{y_{ma}}{2}$, y_{ma}, y_{mi} and $y_{mi} + L_1$. At the wall the shear stress is assumed to be given by the Ludwieg-Tillman law, in the form

$$\tau_W = \tfrac{1}{2}U_{ma}^2\, 0.246(RU_{ma}\theta_{1ma})^{-0.268}\, 10^{-0.678H_{1ma}} \qquad (13)$$

where $\theta_{1ma} = \int_0^{y_{ma}} \frac{U}{U_{ma}}\left(1 - \frac{U}{U_{ma}}\right) dy$

and $H_{1ma} = \frac{1}{\theta_{1ma}} \int_0^{y_{ma}} \left(1 - \frac{U}{U_{ma}}\right) dy$.

The accuracy of the Ludwieg-Tillman law when used in this way is doubtful, but in the large pressure gradients usually present over high-lift aerofoils it is unlikely that small changes in the shear stress will have a significant effect on the calculations. In fact the skin-friction calculations described in section 4 using equation (13) are in fair agreement with experiment and so the errors incurred in calculations of flow development should be small.

At $y = \frac{y_{ma}}{2}$ and $y = y_{mi} + L_1$ the eddy viscosity concept has been used.

At $y = \frac{y_{ma}}{2}$ the kinematic eddy viscosity has been assumed to be given by

$$\frac{\nu_T}{\nu} = \frac{U_{ma}\delta^*_{1ma}}{R_{TB}} R \qquad (14)$$

where ν_T is the kinematic eddy viscosity, δ^*_{1ma} is equal to $\theta_{1ma}H_{1ma}$ and R_{TB} is a dimensionless constant. This expression has been obtained from that used by Cebeci and Smith[8] for the outer part of a turbulent boundary layer. The intermittency factor at the midpoint of the boundary layer has been assumed to be unity. The value of R_{TB} implied by the expression of Cebeci and Smith was 60, and this has been found to give satisfactory agreement with experiment in calculations described in section 4. At $y = y_{mi} + L_1$ the following expression has been used

$$\left(\frac{\nu_T}{\nu}\right) = \frac{(U_e - U_{mi})\hat{L}_1 R_\infty}{R_{TW}} \qquad (15)$$

where R_{TW} is another dimensionless constant. This expression is the same as that suggested by Townsend[9] for self-preserving wakes. The wakes considered here are unlikely to be of this category, but at present there is no proven

equivalent expression that applies to wakes that are not self-preserving. Gartshore[4] has proposed an expression by which the variation of R_{TW} in the streamwise direction may be calculated, but there is little basis at present for assuming it to be any more valid in the conditions considered here than equation (15), which is simpler. The range of values of R_{TW} given by Townsend's theory was between 13 and 18. Since the wakes encountered in the experiments[1] were not self-preserving, it was not surprising that values different from this were required to give satisfactory agreement with experiment in the calculations of section 4.

At the velocity maximum and minimum the eddy viscosity concept would dictate that the shear stress is zero, but there is ample evidence to show that this is not generally true[10,11,12]. However, the shear stress at velocity maxima and minima is usually small compared to the peak values occurring in other parts of the flow, so that in most of the calculations of section 4 it has been assumed to be zero. Only in two cases have τ_{mi} and τ_{ma} been given non-zero values, which were chosen somewhat arbitrarily, so that the effect on the calculation could be seen.

3 COMPARISON WITH EXPERIMENT

3.1 Choosing a method of comparison

The conventional way of assessing the results of an integral method is to compare with experiment the calculated variations of the integral quantities that will be used in making the viscous correction to potential flow calculations, i.e. the momentum and displacement thicknesses. For flows without appreciable static pressure variation across the layer the definitions of the momentum and displacement thicknesses are simple. Myring[13] has examined the case where normal static pressure gradients are significant, and the definitions are more complex, depending on where the momentum or displacement thickness is to be placed in the flow field. However, it is by no means yet clear how the viscous correction is to be incorporated into the potential flow calculations around multi-aerofoil sections. Therefore, at present, attention will be confined to easily calculated integral quantities similar, but not identical to, the momentum and displacement thicknesses. The integral quantities that have been used are defined in Appendix B.

3.2 Experimental data

The pressure distributions and traverse data used in comparing the results of calculations with experiment were obtained during twodimensional wind tunnel

tests on a 0.915m chord wing with a 40% chord slotted flap and plain leading edge at a speed of 61 ms^{-1}. The experiments have been fully described in Ref.1.

To be consistent with the assumptions of the theory, the assumption of linear variation of the static pressure coefficient with normal distance from the surface, was also used in calculating the velocity profiles of the wake and boundary layer from the measured values of total pressure and static pressure in the viscous layer. The position of the maximum in the velocity profile was calculated in the reduction program by fitting a parabola to the point of maximum measured velocity and the two points either side. The velocity minimum was found in a similar way. Integration of the velocity profile to find the values of the integral quantities defined in equations (B-1) to (B-9) was carried out using linear interpolation between the experimental points.

The starting point for the calculation was chosen to be the first traverse position downstream of the slot, where the data was accurate. Although traverses were made in the slot itself the thinness of the boundary layer on the flap and difficulties in 'touching down' the pitot probe on the shroud lower surface caused some uncertainties in interpreting the data.

3.3 Results

The calculation method has been programmed in Fortran making use of the ICL Scientific Subroutine F4MERS to carry out the integration procedure. The starting values of the profile parameters were calculated from the experimental values of the integral quantities defined in equations (B-1) to (B-9), using equations (B-10) to (B-15). Since a region of irrotational flow existed between the wake and boundary layer at the starting point of the calculation it was also necessary to provide the measured value of either L or y_{mi}. The value of y_{mi} was used because it was easier to define from the experimental results.

Before the calculations could proceed it was necessary to decide upon a value of the constant G_0, as defined in section 2. Calculations were carried out for three different values of G_0, 2.30, 2.50 and 2.77, and it was found that the only significant effect was on the value of θ_{2ma}, the momentum thickness of the inner wake. When F, τ_{ma} and τ_{mi} were assumed to be zero the best overall agreement with the experimental variation of θ_{2ma} was with G_0 equal to 2.5 and this was the value used in all the calculations described below.

The results of calculations have been compared with three experimental cases; firstly a case where virtually no interaction occurred between the wake

and boundary layer, secondly where slight interaction occurred and thirdly where the interaction was greater. The results for the first case, assuming F, τ_{ma} and τ_{mi} to be zero, are shown in Figs.7 and 8 for values of R_{TW} equal to 20 and 40. The velocity profiles in Fig.8 show how the lower value of R_{TW}, i.e. higher eddy viscosity, tends to reduce the velocity deficit in the wake. No interaction between the wake and boundary layer was predicted with either value of R_{TW}, and so the boundary-layer development was the same for both. The agreement with the experimental values of θ_{1ma} and H_{1ma} shown in Fig.7 was quite good, except very near to the trailing edge, where the high value of H_{1ma} indicated that the flow was on the point of separating. Since the boundary layer was unaffected by the wake for this case it was of interest to see how the calculated development compared with that by another method for turbulent boundary layers. The results of using Green's method[14], which is an extension of Head's entrainment method[7], are therefore included in Fig.7 and there appears to be very little difference in θ_{1ma} and H_{1ma}. The agreement of the calculated values of θ_{2ma} and θ_{3e} with experiment was not particularly good but improved near to the trailing edge. However, if the sum of θ_{2ma} and θ_{3e} is considered, the difference between experiment and calculation is considerably reduced, which suggests that inaccuracy in determining the measured value of y_{mi} might be partly to blame. It is worth noting that the variation of R_{TW} had little effect on θ_{2ma} and θ_{3e}, in contrast with its effect on H_{2ma} and H_{3e}. It appears possible to obtain good agreement with the experimental variation of H_{2ma} and H_{3e} by choosing the right value of R_{TW}.

Still keeping F, τ_{mi} and τ_{ma} zero and with R_{TW} equal to 40, the results for the slightly interacting case are shown in Figs.9 and 10. The agreement with the measured integral quantities was quite good, but the interaction between the wake and boundary layer was predicted to commence at $\bar{x}$ equal to 0.317, whereas the measured profiles in Fig.10 indicate that some interaction was present even at $\bar{x}$ equal to 0.204. This was considered to be largely due to the departure from a Gaussian profile in the inner half wake, owing to the presence of a separation bubble on the lower surface of the wing near to its trailing edge. This feature was not so noticeable in the previous case, where a slightly modified shape of wing lower surface was used. The effect was more evident at an angle of incidence lower than the 8° of this case, as is shown by the total head profiles, particularly that at the slot, in Fig.1, for which the angle of incidence was zero. The effect of the bubble was to add to the inner edge of the wake a turbulent layer of small total head deficit, which

interacted with the boundary layer before the main part of the wake. This effect can be seen in Fig.10. The point at which the boundary layer separated was estimated, by examination of the experimental pressure distributions on the flap surface, to be at $\bar{x}$ equal to 0.305, where the calculated value of H_{1ma} was about 1.9. Since the wake had only interacted very weakly with the boundary layer up to this station it seems likely that the boundary layer would have separated at this point even without the presence of the wake.

In the third case the slot width had been reduced from 0.025c to 0.020c with otherwise the same model configuration as for the second case. The wake and boundary-layer interaction was still not very severe although greater than in the two previous cases. The results, still keeping F, τ_{ma} and τ_{mi} equal to zero, and with R_{TW} equal to 40, are shown (C_p varying) in Figs.11 and 12, compared with experiment. Although the agreement with integral quantities was quite good, the point at which interaction commenced, $\bar{x}$ equal to 0.256, was again further downstream than the position indicated by the measured velocity profiles. The bubble on the wing lower surface was once more considered to be the cause of this. The calculated velocity profiles in Fig.12 show the interaction to be more severe than in the previous case (Fig.10) but again, by reference to the velocity at the edge of the boundary layer, not quite as severe as in the experiments. The point where the boundary layer separated, again determined from the measured pressure distribution, was at $\bar{x}$ equal to 0.340 where the calculated value of H_{1ma} was 2.0 approximately.

In Fig.13 the calculated skin friction for the above three cases is compared with values measured using surface pitot tubes. The measurements, which have been described in Ref.1, were made using a circular pitot tube for the first case and a rectangular one for the remaining two. The agreement for the non-interacting case in Fig.13a is certainly no better than for the interacting cases in Figs.13b and 13c, giving some justification for using the Ludwieg-Tillman expression in the form given by equation (13). In Fig.13a the result of using the Green-Head method[14] is also included and it can be seen to be in close agreement with the present method.

In the calculations described so far the values of τ_{ma}, τ_{mi} and F have all been zero, and the agreement with experiment could be generally described as quite good. It is of interest, however, to see how non-zero values of these quantities affect the results, and also to see the effect of ignoring the variation of static pressure normal to the surface. The latter is shown in

Fig.11 for the third of the above three cases. The static pressure through both the boundary layer and the wake was assumed to be equal to that at the surface and the effect can be seen to be quite large. This implies that pressure variations normal to the surface should be included in the calculations.

In Fig. 14 the effects of non-zero values of τ_{mi} and τ_{ma} are shown for the same case. The choice of values for τ_{mi} and τ_{ma} has, of necessity, been somewhat arbitrary. However, as a guide, use has been made of the hot wire measurements of English[10] which showed both τ_{mi} and τ_{ma} to be predominantly negative. Thus τ_{mi} has been put equal to $-\frac{1}{2}\tau_{L1}$ and τ_{ma} equal to $-\frac{1}{2}\tau_{ma2}$. First, keeping τ_{ma} zero, Fig.14 shows the negative value of τ_{mi} to have a marked effect on the integral quantities of the inner half wake where it substantially reduced both θ_{2ma} and H_{2ma}. Since it caused considerable departure from the experimental values it appears that in the real flow the negative value of τ_{mi} was less in magnitude than $-\frac{1}{2}\tau_{L1}$. The effects on the outer half wake and boundary layer were smaller. With both τ_{mi} and τ_{ma} non-zero little further change occurred in the wake but the value of θ_{1ma} was increased substantially. The effect on the velocity profile is shown in Fig.12 to be a tendency to eliminate the velocity maximum and minimum.

In Fig.15 the results of the calculation are shown with τ_{ma} and τ_{mi} zero but with F given by equation (12). In Fig.16 the variation of the mass-flow below y equal to y_{mi} in the calculation is compared with experiment and with the constant massflow resulting when F is zero. It can be seen that equation (12) gives a more accurate variation of the massflow than assuming F is zero but agreement with the experimental values of the integral quantities in Fig.15 is not significantly improved.

The data used above was obtained during experiments[1] in which the aim was to discover the particular features of the flow over an aerofoil with a slotted flap that lead to optimum performance. The optimum was quite sensitive to slot width, lying in the range 0.020c to 0.025c for the Reynolds number of the tests ($R = 3.8 \times 10^6$), which was also the range where the wake began to affect the boundary layer, as is shown by the velocity profiles in Figs.10 and 12. It is of interest, therefore, to carry out the calculation for a smaller slot size. However, the only slot size less than 0.020c at which boundary layer traverses were made was at 0.005c, where the flow separated from the flap just downstream of the slot exit, making a useful comparison with experiment impossible. Therefore, a hypothetical case has been calculated for a slot width smaller than

0.020c. To do this the same starting values and pressure distribution as for the 0.020c case were used, except that the wake was moved nearer to the surface, so that interaction commenced at the starting station ($\bar{x} = 0.114$). This corresponded to a slot size of approximately 0.015c. For comparison the same calculation was carried out with the wake moved away far enough for there to be no interaction at all. The values of F, τ_{ma} and τ_{m1} we all set to zero. The results for the boundary layer are shown in Fig.17 and it can be seen that H_{1ma} increased much faster in the interacting case, which can be interpreted as indicating an earlier separation of the flow from the flap upper surface.

4 DISCUSSION

The results in the previous section show that the calculation method gives quite good predictions of the integral properties of the wake and boundary layer, and in a non-interacting case the results for the boundary layer were very similar to those obtained by the Green-Head method[14]. In the two interacting cases for which data was available it predicted less severe interactions than those observed, but this was considered to be largely attributable to the effects of the bubble on the wing lower surface. In the hypothetical case where the interaction was strong the calculations predicted that an earlier separation of the boundary layer would occur because of the effect of the wake.

It is worth noting that in the experiments[1] the pressure distribution on the flap was not very sensitive to changes in slot width, except when the latter became very small. Thus, the pressure data used in the hypothetical cases were probably only slightly different from the pressures in the equivalent real flows. It follows that the starting values of θ_{1ma} and H_{1ma} that were used would have been close to those in the equivalent real flows. (Transition occurred very near to the flap leading edge for the flap deflections of 30° and thus would have been unaffected by the irrotational disturbances from the wake discussed in Ref.1.) Some change in the size of the wake was to be expected, owing to the slightly different load being carried by the wing, in changing the slot width from 0.020c to approximately 0.015c; but assuming that this change in size was small compared to the distance (0.005c approximately) by which the wake was moved closer to the flap, this would not have had a large effect on the calculation of the boundary layer development. There is some justification, therefore, for saying that the calculation of the hypothetical strongly-interacting case was carried out in conditions close to those in the equivalent real flow. Comparing now the non-interacting case in Fig.17 with the slightly-interacting case (F = 0) in Fig.15, the calculated development of the boundary

layer was very similar in both cases, i.e. at the slot width of 0.020c the calculation predicted that, even though some interaction occurred, it did not significantly affect the integral properties of the boundary layer. However, the calculations indicated that between the slot widths of 0.020c and 0.015c approximately the wake began to have a significant effect on the boundary layer and that the position of separation began to move upstream. This coincided with the beginning of the observed fall-off in performance of the wing/flap combination in the experiments[1].

Considering some possible improvements of the calculation method, it would be most useful if a valid expression for F, the massflow rate across the velocity minimum in the wake, could be obtained near to the trailing edge of the wing. Such an expression would enable calculations to start very near to or perhaps even at the slot exit. It is likely that in a very strongly interacting case the approximation that F is zero would not be a very good one, and so further knowledge of the variation of F in this situation would be useful. There is also the possibility that more sophisticated assumptions regarding the shear stress could be made, although this will have to await a more detailed understanding of the turbulence structure of wakes and boundary layers.

The limitations of the method are those that apply to integral methods generally, in that they can only be used successfully where the streamwise component of velocity can be represented accurately by a certain family of velocity profiles. In this case it was found that a separation bubble on the lower surface of the wing caused some deviation of the velocity in the wake from the assumed Gaussian form, and this resulted in slightly stronger interaction with the boundary layer than that indicated by the calculations. Also, as it stands, the method is not suited to the region downstream of the point where the velocity maximum disappears. For the flow over a flap this is unlikely to be a serious limitation because it has been shown in Ref.1 that, when the flap is near to its optimum position, the interaction between the wake and boundary layer is weak, which implies that a velocity maximum is still present at the flap trailing edge. If the slot width is much smaller than the optimum, the calculation will indicate this by predicting a strong interaction. However, if the turbulent flow over the wing with a slatted leading edge is to be calculated, where the wake and boundary layer usually interact strongly near to the optimum configuration, a differential method would be more suitable. This also applies to the turbulent flow over multiple-slotted flaps where more than one wake is present.

5 CONCLUSIONS

An integral method has been developed for calculating the turbulent flow over a slotted flap. The effect of the static pressure variation normal to the flap surface is included and account is taken of the interaction between the wake and boundary layer. It gives some idea as to the extent of the interaction of the wake and boundary layer and predicts an earlier separation of the boundary layer when the effect of the wake is large. When the wake has no effect the results for the boundary layer are very close to those obtained using the Green-Head method [14].

Appendix A

DERIVATION AND SOLUTION OF THE EQUATIONS

The momentum equation of the viscous layer equations (4) is integrated in the direction normal to the surface between the arbitrary limits $y = y_1$ and $y = y_2$. If the continuity equation (6) is used, this gives

$$\frac{d}{dx}\int_{y_1}^{y_2} U^2 dy - U_2 \frac{d}{dx}\int_0^{y_2} U dy + U_1 \frac{d}{dx}\int_0^{y_1} U dy + \frac{1}{2}\int_{y_1}^{y_2} \frac{\partial C_{p(y)}}{\partial x} dy - (\tau_2 - \tau_1) = 0 \quad \ldots. \text{(A-1)}$$

where U_1 and U_2 are the values of U at y_1 and y_2 respectively and τ_1 and τ_2 are the corresponding values of τ. The assumed velocity profiles can be substituted into equation (A-1) to obtain the required equations. The model has to deal with two distinct physical situations; the case where the boundary layer and wake are separated by a region of irrotational flow and the case where the boundary layer and wake are merged. A set of equations will be derived for each case.

This distinction does not apply to the outer half of the wake, thus substituting the assumed profile into equation (A-1) for two intervals in the wake will give results having general applicability. For $y_1 = y_{mi}$, $y_2 = y_{mi} + G_1 L_1$

$$\frac{dU_{mi}}{dx} C_1 + \frac{dL_1}{dx} C_2 = \frac{dU_e}{dx} C_3 + P_5 + C_9 F - \tau_{mi} \qquad \text{(A-2)}$$

for $y_1 = y_{mi}$, $y_2 = y_{mi} + L_1$

$$\frac{dU_{mi}}{dx} C_4 + \frac{dL_1}{dx} C_5 = \frac{dU_e}{dx} C_6 + P_4 + C_{14} F + (\tau_{L1} - \tau_{mi}) \qquad \text{(A-3)}$$

where the coefficients C_i and P_i are defined in Appendix C; τ_{mi}, τ_{L1} are the nondimensional shear stresses at y equal to y_{mi} and $y_{mi} + L_1$ respectively, and F is the rate of change of massflow in the region $0 < y < y_{mi}$. Equations (A-2) and (A-3) can be rearranged to give two equations applicable to the merged and unmerged conditions:

$$\frac{dL_1}{dx} = \frac{1}{(C_5C_1 - C_2C_4)}\left[\frac{dU_e}{dx}(C_1C_6 - C_4C_3) + P_4C_1 - P_5C_4 + (C_1C_{14} - C_9C_4)F + \tau_{L1}C_1 - \tau_{mi}(C_1 - C_4)\right] \quad (A-4)$$

$$\frac{dU_{mi}}{dx} = \frac{1}{C_1}\left[\frac{dU_e}{dx}C_3 + P_5 + C_9F - \tau_{mi} - \frac{dL_1}{dx}C_2\right] . \quad (A-5)$$

Now returning to the integral of the momentum equation (A-1), substitution of the velocity profiles for the inner wake and boundary layer of the merged case can be made. For $y_1 = (y_{mi} - G_0L_0)$, $y_2 = y_{mi}$

$$\frac{dU_{ma}}{dx}C_7 + \frac{dL_0}{dx}C_8 = \frac{dU_{mi}}{dx}C_{10} + P_3 + C_{17}F + (\tau_{mi} - \tau_{ma}) \quad (A-6)$$

for $y_1 = y_{ma}/2$, $y_2 = y_{ma}$

$$\frac{dy_{ma}}{dx}C_{11} + \frac{dn}{dx}C_{12} = \frac{dU_{ma}}{dx}C_{13} + P_2 + (\tau_{ma} - \tau_{ma2}) \quad (A-7)$$

for $y_1 = 0$, $y_2 = y_{ma}$

$$\frac{dy_{ma}}{dx}C_{15} + \frac{dn}{dx}C_{16} = \frac{dU_{ma}}{dx}C_{18} + P_1 + (\tau_{ma} - \tau_W) \quad (A-8)$$

where τ_W, τ_{ma2}, τ_{ma} are the shear stresses at y equal to zero, $y_{ma}/2$, y_{ma}. The set of equations is completed by substitution of the velocity profile into the equation for the rate of change of massflow in the region below the velocity minimum, i.e. $F = \frac{d}{dx}\int_0^{y_{mi}} U dy$.

$$\frac{dy_{ma}}{dx}C_{19} + \frac{dn}{dx}C_{20} = \frac{dU_{ma}}{dx}C_{21} + \frac{dU_{mi}}{dx}C_{22} + \frac{dL_0}{dx}C_{23} + F . \quad (A-9)$$

Appendix A

The four equations ((A-6) to (A-9)) can be rearranged to give

$$\frac{dy_{ma}}{dx} = \frac{1}{(b_1b_6 - b_5b_2)}\left[\frac{dU_{mi}}{dx}(b_4b_6 - b_8b_2) - P_1b_2 + P_2b_6 + P_3(b_6b_3 - b_7b_2) + (b_9b_6 - b_{10}b_2)F + (\tau_{mi} - \tau_{ma})(b_3b_6 - b_7b_2) + (\tau_{ma} - \tau_{ma2})b_6 - (\tau_{ma} - \tau_W)b_2\right] \quad \text{(A-10)}$$

$$\frac{dn}{dx} = \frac{1}{b_6}\left[\frac{dU_{mi}}{dx}b_8 - \frac{dy_{ma}}{dx}b_5 + P_1 + P_3b_7 + b_{10}F + (\tau_{mi} - \tau_{ma})b_7 + (\tau_{ma} - \tau_W)\right] \quad \text{(A-11)}$$

$$\frac{dU_{ma}}{dx} = \frac{1}{(C_8C_{21} - C_7C_{23})}\left[\frac{dy_{ma}}{dx}C_{19}C_8 - \frac{dU_{mi}}{dx}(C_{22}C_8 + C_{10}C_{23}) + \frac{dn}{dx}C_{20}C_8 - P_3C_{23} - (C_8 + C_{23}C_{17})F - (\tau_{mi} - \tau_{ma})C_{23}\right] \quad \text{(A-12)}$$

$$\frac{dL_0}{dx} = \frac{1}{C_8}\left[\frac{dU_{mi}}{dx}C_{10} + P_3 + C_{17}F + (\tau_{mi} - \tau_{ma}) - \frac{dU_{ma}}{dx}C_7\right] \quad \text{(A-13)}$$

where b_i are defined in Appendix C.

These four equations taken with equations (A-4), (A-5) formed a complete set of equations for the unknowns U_{ma}, y_{ma}, n, U_{mi}, L_0, L_1. They can be integrated in the downstream direction by a standard computer program. The program used in this case was Merson's method, which varies the step length to keep errors within specified limits and is available in ICL Scientific Subroutine F4MERS.

For the case where the wake and boundary layer are separated by a region of irrotational flow, the equations derived from the substitution of the velocity profiles in the inner wake and boundary layers into equation (A-1) can be rearranged to give:

$$\frac{dL_0}{dx} = \frac{1}{C_8}\left[\frac{dU_{mi}}{dx} C_{10} + P_3 + C_{17}F + (\tau_{mi} - \tau_{ma}) - \frac{dU_{iW}}{dx} C_7\right] \qquad (A\text{-}14)$$

$$\frac{dn}{dx} = \frac{1}{(C_{11}C_{16} - C_{12}C_{15})}\left[\frac{dU_{iB}}{dx}(C_{18}C_{11} - C_{13}C_{15}) + P_1C_{11} - P_2C_{15} + (\tau_{ma} - \tau_W)C_{11} - (\tau_{ma} - \tau_{ma2})C_{15}\right] \qquad (A\text{-}15)$$

$$\frac{dy_{ma}}{dx} = \frac{1}{C_{11}}\left[\frac{dU_{iB}}{dx} C_{13} + P_2 + (\tau_{ma} - \tau_{ma2}) - \frac{dn}{dx} C_{12}\right] \qquad (A\text{-}16)$$

where U_{iW} is the 'inviscid' velocity at the edge of the inner half wake and U_{iB} that at the edge of the boundary layer.

The shear stress τ_{ma} has been left in the above equations, although when the wake and boundary layer are separate its value would be expected to be zero. Again the equation for the rate of change of massflow in the region below the velocity minimum provides the final equation.

$$\frac{dL}{dx} = \frac{2}{(U_{iW} + U_{iB})}\left\{-\frac{dy_{ma}}{dx} C_{19} - \frac{dn}{dx} C_{20} + \frac{dL_0}{dx} C_{23} + \frac{dU_{mi}}{dx} C_{22} + \frac{dU_{iW}}{dx}\left(-L_0(G_0 - K_5) - \frac{L}{2}\right) + \frac{dU_{iB}}{dx}\left(-\frac{y_{ma}}{n+1} - \frac{L}{2}\right) + F\right\} . \qquad (A\text{-}17)$$

Equations (A-14) to (A-17) with equations (A-4), (A-5) form the complete set for the unmerged case, where the variables are L, y_{ma}, n, U_{mi}, L_0, L_1. This set is solved in the manner indicated above.

If the calculation starts in the unmerged condition the value of L is examined at the end of each integration step, until it is anticipated that it will become negative or zero at the end of the next step. The point at which it becomes zero is then calculated, together with values of the other five profile parameters there, and the calculation procedure then recommences using the equations for the merged condition.

Appendix B

DEFINITION OF INTEGRAL QUANTITIES

$$\delta^*_{1ma} = \int_0^{y_{ma}} \left(1 - \frac{U}{U_{ma}}\right) dy \tag{B-1}$$

$$\theta_{1ma} = \int_0^{y_{ma}} \frac{U}{U_{ma}} \left(1 - \frac{U}{U_{ma}}\right) dy \tag{B-2}$$

$$H_{1ma} = \delta^*_{1ma}/\theta_{1ma} \tag{B-3}$$

where $U_{ma} = U_{iB}$ when the wake and boundary layer are separate.

$$\delta^*_{2ma} = \int_{y_{mi}-G_0L_0}^{y_{m1}} \left(1 - \frac{U}{U_{ma}}\right) dy \tag{B-4}$$

$$\theta_{2ma} = \int_{y_{mi}-G_0L_0}^{y_{mi}} \frac{U}{U_{ma}} \left(1 - \frac{U}{U_{ma}}\right) dy \tag{B-5}$$

$$H_{2ma} = \delta^*_{2ma}/\theta_{2ma} \tag{B-6}$$

where $U_{ma} = U_{iW}$ when the wake and boundary layer are separate.

$$\delta^*_{3e} = \int_{y_{mi}}^{y_{mi}+G_1L_1} \left(1 - \frac{U}{U_e}\right) dy \tag{B-7}$$

$$\theta_{3e} = \int_{y_{mi}}^{y_{mi}+G_1L_1} \frac{U}{U_e} \left(1 - \frac{U}{U_e}\right) dy \tag{B-8}$$

$$H_{3e} = \delta^*_{3e}/\theta_{3e} \ . \tag{B-9}$$

On substituting the assumed velocity profiles into these equations we obtain the relationships between the parameters describing the assumed velocity profiles and the integral quantities as:

$$H_{1ma} = 2n + 1 \tag{B-10}$$

$$\delta^*_{1ma} = \frac{n}{n+1} y_{ma} \tag{B-11}$$

$$H_{2ma} = \frac{1}{\left(1 - \frac{K_6}{K_5}\left(1 - \frac{U_{mi}}{U_{ma}}\right)\right)} \tag{B-12}$$

$$\delta^*_{2ma} = L_0 K_5 \left(1 - \frac{U_{mi}}{U_{ma}}\right) \tag{B-13}$$

$$H_{3e} = \frac{1}{\left(1 - \frac{K_2}{K_1}\left(1 - \frac{U_{mi}}{U_e}\right)\right)} \tag{B-14}$$

$$\delta^*_{3e} = L_1 K_1 \left(1 - \frac{U_{mi}}{U_e}\right) \tag{B-15}$$

where K_1, K_2, K_5 and K_6 are constants given in Appendix C. When the wake and boundary layer are separate U_{ma} is replaced by U_{iW} in equations (B-12) and (B-13).

Appendix C

COEFFICIENTS OF APPENDICES A AND B

The coefficients are:-

$$C_1 = -L_1\left(U_e(2K_2 - K_1) - 2U_{mi}K_2\right)$$

$$C_2 = (U_e - U_{mi})\left(U_e(K_2 - K_1) - U_{mi}K_2\right)$$

$$C_3 = -L_1\left(U_e(G_1 + 2K_2 - 3K_1) + 2U_{mi}(K_1 - K_2)\right)$$

$$C_4 = L_1\left((U_e - U_{mi})\left(\frac{K_3}{2} - 2K_4\right) + U_eK_3\right)$$

$$C_5 = (U_e - U_{mi})^2\left(K_4 - \frac{K_3}{2}\right) - (U_e - U_{mi})U_e\left(K_3 - \frac{1}{2}\right)$$

$$C_6 = L_1\left(\left(\frac{5}{2}K_3 - 2K_4 - \frac{1}{2}\right)(U_e - U_{mi}) + U_e(K_3 - 1)\right)$$

$$C_7 = L_0\left(U_{ma}(G_0 - 3K_5 + 2K_6) + 2U_{mi}(K_5 - K_6)\right)$$

$$C_8 = (U_{ma} - U_{mi})\left(U_{ma}(K_6 - K_5) - U_{mi}K_6\right)$$

$$C_9 = U_e - U_{mi}$$

$$C_{10} = L_0\left(U_{ma}(2K_6 - K_5) - 2U_{mi}K_6\right)$$

$$C_{11} = -U_{ma}^2 nW$$

$$C_{12} = U_{ma}^2 y_{ma}\left(\frac{(2n^2 - 1)W}{(2n + 1)(n + 1)} + \ln 2\left(\frac{1}{(2n + 1)(n + 1)} - W\right)\right)$$

$$C_{13} = -U_{ma}y_{ma}W$$

$$C_{14} = \frac{U_e - U_{mi}}{2}$$

$$C_{15} = -\frac{U_{ma}^2 n}{(2n + 1)(n + 1)}$$

$$C_{16} = \frac{U_{ma}^2 y_{ma}(2n^2 - 1)}{(2n + 1)^2(n + 1)^2}$$

$$C_{17} = -(U_{ma} - U_{mi})$$

$$C_{18} = -\frac{U_{ma} y_{ma}}{(2n + 1)(n + 1)}$$

$$C_{19} = \frac{U_{ma}}{n + 1} \quad *$$

$$C_{20} = -\frac{U_{ma} y_{ma}}{(n + 1)^2} \quad *$$

$$C_{21} = -L_0(G_0 - K_5) - \frac{y_{ma}}{(n + 1)}$$

$$C_{22} = -L_0 K_5$$

$$C_{23} = -U_{ma}(G_0 - K_5) - U_{mi} K5^{**}$$

where $K_1 = \int_0^{G_1} \exp(-k\eta^2)d\eta = 1.0633$

$K_2 = \int_0^{G_1} \exp(-2k\eta^2)d\eta = 0.7526$

} for $G_1 = 2.77$

$$K_3 = \int_0^1 \exp(-k\eta^2)d\eta = 0.8101$$

$$K_4 = \int_0^1 \exp(-2k\eta^2)d\eta = 0.6805$$

---

* In unmerged case U_{ma} is replaced by U_{iB}.

** In unmerged case U_{ma} is replaced by U_{iW}.

$$\left.\begin{aligned} K_5 &= \int_{-G_0}^{0} \exp(-k\eta^2)d\eta = 1.0610 \\ K_6 &= \int_{-G_0}^{0} \exp(-2k\eta^2)d\eta = 0.7526 \end{aligned}\right\} \text{ for } G_0 = 2.50$$

$$W = \frac{1 - (\tfrac{1}{2})^{2n+1}}{(2n+1)(n+1)} \quad .$$

When the wake and boundary layer are separated by a region of irrotational flow U_{ma} is replaced in C_7, C_8, C_{10}, C_{17} and C_{23} by U_{iW} and in C_{11}, C_{12}, C_{13}, C_{15}, C_{16}, C_{18}, C_{19} and C_{20} by U_{iB}.

The coefficients b are given by:-

$$b_1 = C_{11} - \frac{C_{13}C_{19}C_8}{A}$$

$$b_2 = C_{12} - \frac{C_{13}C_{20}C_8}{A}$$

$$b_3 = - \frac{C_{13}C_{23}}{A}$$

$$b_4 = - (C_{22}C_8 + C_{10}C_{23}) \frac{C_{13}}{A}$$

$$b_5 = C_{15} - \frac{C_{18}C_{19}C_8}{A}$$

$$b_6 = C_{16} - \frac{C_8C_{20}C_{18}}{A}$$

$$b_7 = - \frac{C_{18}C_{23}}{A}$$

$$b_8 = - (C_{22}C_8 + C_{10}C_{23}) \frac{C_{18}}{A}$$

$$b_9 = -\frac{C_{13}}{A}(C_8 + C_{23}C_{17})$$

$$b_{10} = -\frac{C_{18}}{A}(C_8 + C_{23}C_{17})$$

where $A = C_8C_{21} - C_7C_{23}$.

The pressure terms P_i $(i = 1,5)$ are given by

$$P_i = -\frac{1}{2}\int_{y_1}^{y_2} \frac{\partial C_{p(y)}}{\partial x}\, dy$$

where y_1 and y_2 take the values given in the table below.

i	y_1	y_2
1	0	y_{ma}
2	$y_{ma}/2$	y_{ma}
3	$y_{mi} - G_0L_0$	y_{mi}
4	y_{mi}	$y_{mi} + L_1$
5	y_{mi}	$y_{mi} + G_1L_1$

SYMBOLS

b_i $i = 1$ to 10	see Appendix
C_i $i = 1$ to 23	see Appendix
c	reference length (basic wing-section chord)
c_{f_∞}	skin-friction coefficient $(2\tau_W)$
C_p	static pressure coefficient
F	$\frac{d}{dx}\int_0^{y_{mi}} U dy$
F_s	scaling factor, (equation (12))
G_0, G_1	constants determining the width of the wake
H_{1ma}, H_{2ma}, H_{3e}	form parameters defined in section 4.1
H	total head
k	constant equal to ln 2
K_i $i = 1$ to 6	constants given in the Appendix
L	width of irrotational region between the wake and boundary layer
L_0, L_1	length parameters for the wake (see Fig.2)
n	exponent for the power law for the velocity in the boundary layer
P_∞	reference pressure
P_i $i = 1$ to 5	pressure terms given in the Appendix
R	Reynolds number, $\frac{U_\infty C}{\nu}$
R_{TB}, R_{TW}	dimensionless constants given in section 2.4
U_∞	reference velocity in the free stream
U	streamwise component of velocity divided by U_∞
U_i	the nondimensional 'inviscid' velocity equal to $\sqrt{1 - C_p}$
U_e	the value of U_i at the outer edge of the wake
U_{iB}	the value of U_i at the edge of the boundary layer
U_{iW}	the value of U_i at the inner edge of the wake

SYMBOLS (concluded)

U_{ma}	the value of U at the velocity maximum
U_{mi}	the value of U at the velocity minimum
V	normal component of velocity divided by U_∞
x	streamwise coordinate divided by c
$\bar{x}$	coordinate parallel to flap chord line divided by c
y	coordinate normal to stream divided by c
y_{ma}	the value of y at the velocity maximum
y_{mi}	the value of y at the velocity minimum
α	angle of incidence of wing
δ^*_{1ma}, δ^*_{2ma}, δ^*_{3e}	integral thicknesses defined in section 4.1
θ_{1ma}, θ_{2ma}, θ_{3e}	integral thicknesses defined in section 4.1
κ	curvature of wall
ν	kinematic viscosity
ν_T	kinematic eddy viscosity
τ	shear stress divided by ρU_∞^2
τ_W, τ_{mi}, τ_{ma}, τ_{ma2}, τ_{L1}	values of τ at y equal to zero, y_{mi}, y_{ma}, $y_{ma}/2$ and $y_{mi} + G_1 L_1$ respectively

REFERENCES

No.	Author	Title, etc.
1	D.N. Foster H.P.A.H. Irwin B.R. Williams	The twodimensional flow around a slotted flap. ARC R & M 3681 (1970)
2	I.S. Gartshore B.G. Newman	The turbulent wall jet in an arbitrary pressure gradient. Aeronautical Quarterly, Vol.XX (1969)
3	A.A. Townsend	The mechanism of entrainment in free turbulent flows. J. Fluid. Mech., Vol.26, Part 4 (1966)
4	I.S. Gartshore	Twodimensional turbulent wakes. J. Fluid. Mech., Vol.30, Part 3 (1967)
5	S. Goldstein (Ed)	Modern Developments in Fluid Dynamics. Clarendon Press (1938)
6	J.L. Hess A.M.O. Smith	Calculation of potential flow about arbitrary bodies. Progress in Aeronautical Sciences, Vol.8, 1, 138. Pergamon Press, London (1966)
7	M.R. Head	Entrainment in the turbulent boundary layer. ARC R & M 3152 (1958)
8	T. Cebeci A.M.O. Smith	A finite difference method for calculating laminar and turbulent boundary layers. J. Basic Engineering, September 1970
9	A.A. Townsend	The structure of turbulent shear flow. Cambridge University Press (1956)
10	E.C. English	Ph.D. Thesis, Cambridge University (1970)
11	P. Bradshaw M.J. Gee	Turbulent wall jets with and without an external stream. ARC R & M 3252 (1960)
12	J.O. Hinze	Turbulent flow regions with shear stress and mean velocity gradient of opposite sign. App. Sci. Res., 22, May 1970

REFERENCES (concluded)

No.	Author	Title, etc.
13	D.F. Myring	The effects of normal pressure gradients on the boundary layer momentum integral equation. RAE Technical Report 68214 (ARC 30858) (1968)
14	J.E. Green	Application of Head's entrainment method to the prediction of turbulent boundary layers and wakes in compressible flow. RAE Technical Report 72079 (ARC 34052) (1972)

Table 1 - VARIATION OF CURVATURE ABOVE FLAP SURFACE

Inviscid				Viscous				
$\frac{\partial C_p}{\partial y} = 5.79$				$\frac{\partial C_p}{\partial y} = 4.45$				
y	C_p	u^2	κ	y	C_p	u^2	κ	Position 1 $\bar{x} = 0.11$
0.0	-1.698	2.69	1.08	0.00267	-1.236	2.132	1.05	
0.02	-1.609	2.61	1.11	0.02008	-1.157	1.421	1.57	
0.04	-1.467	2.47	1.17	0.04990	-1.025	2.017	1.10	
0.06	-1.341	2.34	1.24	0.05811	-0.989	1.986	1.12	
0.08	-1.235	2.23	1.29					
0.10	-1.148	2.15	1.35					
$\frac{\partial C_p}{\partial y} = 4.6$				$\frac{\partial C_p}{\partial y} = 1.98$				
0.0	-1.2017	2.202	1.045	0.00072	-0.724	1.113	0.89	Position 2 $\bar{x} = 0.204$
0.02	-1.0821	2.082	1.105	0.02182	-0.69	1.17	0.847	
0.04	-0.9834	1.983	1.159	0.04897	-0.63	1.362	0.728	
0.06	-0.9019	1.902	1.209	0.07607	-0.58	1.575	0.629	
0.08	-0.8337	1.834	1.254					
0.10	-0.7763	1.776	1.295					
$\frac{\partial C_p}{\partial y} = 1.82$				$\frac{\partial C_p}{\partial y} = 0.087$				
0.0	-0.6051	1.6051	0.566	0.00163	-0.29	0.340	0.129	Position 3 $\bar{x} = 0.281$
0.02	-0.5799	1.5799	0.575	0.02339	-0.29	0.875	0.050	
0.04	-0.5280	1.5280	0.595	0.04808	-0.29	0.561	0.078	
0.06	-0.4889	1.4889	0.611	0.09371	-0.30	1.296	0.034	
0.08	-0.4596	1.4596	0.623					
0.10	-0.4372	1.4372	0.632					
$\frac{\partial C_p}{\partial y} = -1.8$				$\frac{\partial C_p}{\partial y} = -1.2$				
0.0	0.1825	0.8175	-1.10	0.00624	0.06	0.047	-12.81	Position 4 $\bar{x} = 0.376$
0.02	0.1175	0.8825	-1.02	0.04412	0.01	0.439	-1.371	
0.04	0.0775	0.9225	-0.976	0.07750	-0.03	0.371	-1.623	
0.06	0.0391	0.9609	-0.937	0.1135	-0.07	1.071	-0.562	
0.08	0.0066	0.9934	-0.906					
0.10	-0.0205	1.0205	-0.882					

Table 2

COMPARISON OF STREAMLINE CURVATURES

Position 1 $\bar{x}$ = 0.114

	Curvature necessary to maintain the static pressure variation	Curvature of streamline: calculated by fitting a cubic polynomial along each streamline
y	κ	κ
0.00267	1.05	2.5
0.02	1.57	2.5
0.05	1.10	1.7
0.058	1.12	0.6

Position 2 $\bar{x}$ = 0.204

0.00272	0.89	1.2
0.022	0.85	0.9
0.049	0.73	0.5
0.076	0.63	0.12

Position 3 $\bar{x}$ = 0.281

0.00163	0.129	0.477
0.023	0.050	0.005
0.048	0.078	-0.28
0.094	0.034	-0.28

Position 4 $\bar{x}$ = 0.376

0.00624	-12.8	-0.23
0.044	-1.37	-1.2
0.078	-1.62	-1.5
0.1135	-0.56	-0.9

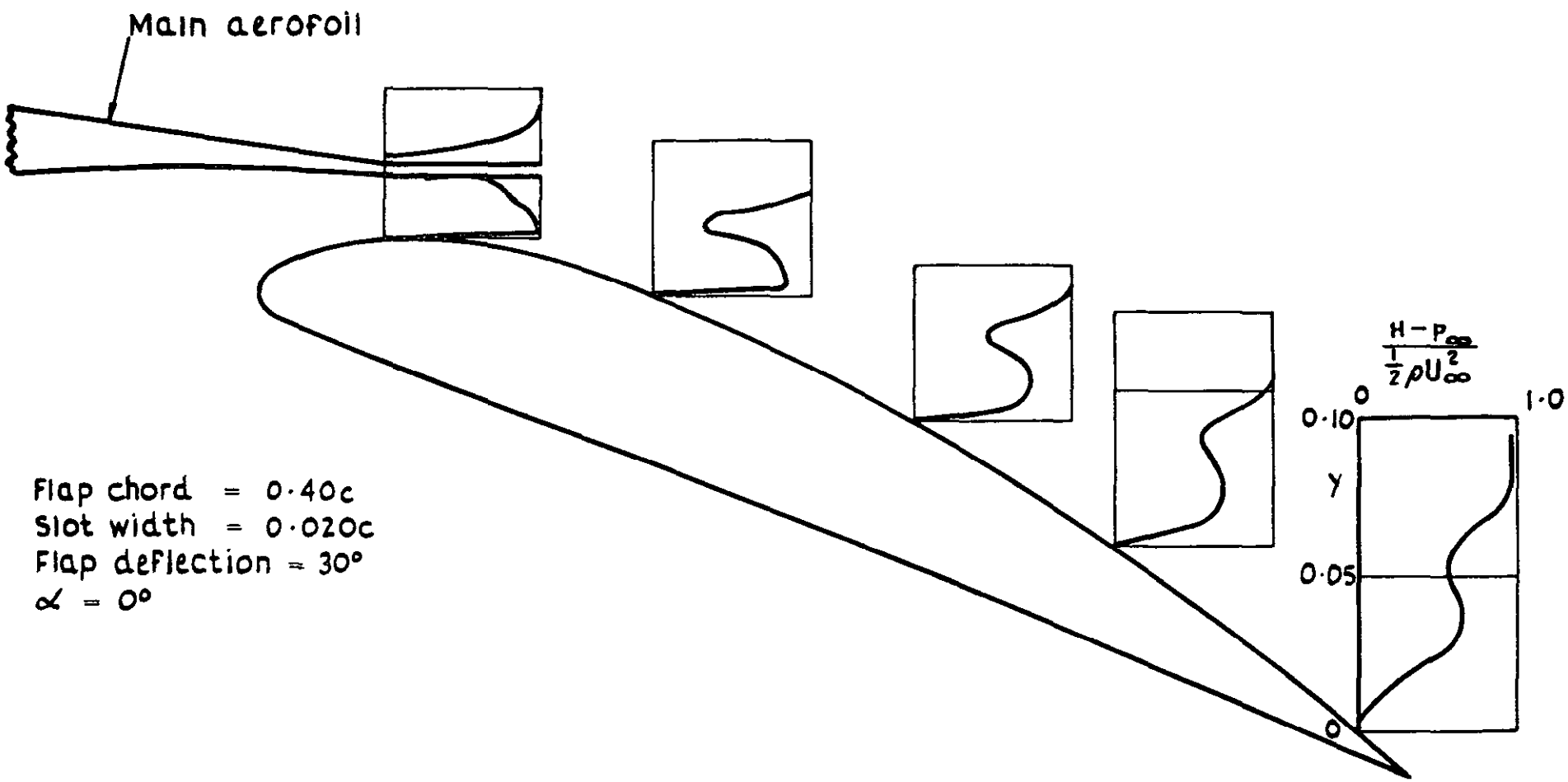

Fig. 1 Example of measured total head profiles

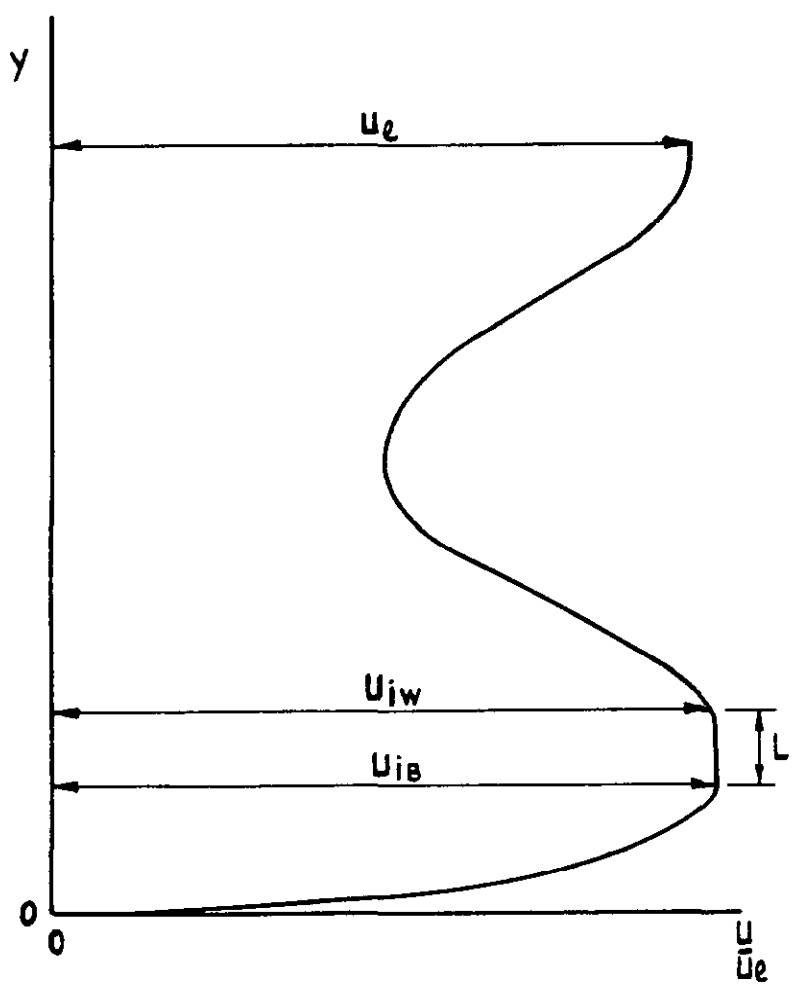

a Wake and boundary layer separate

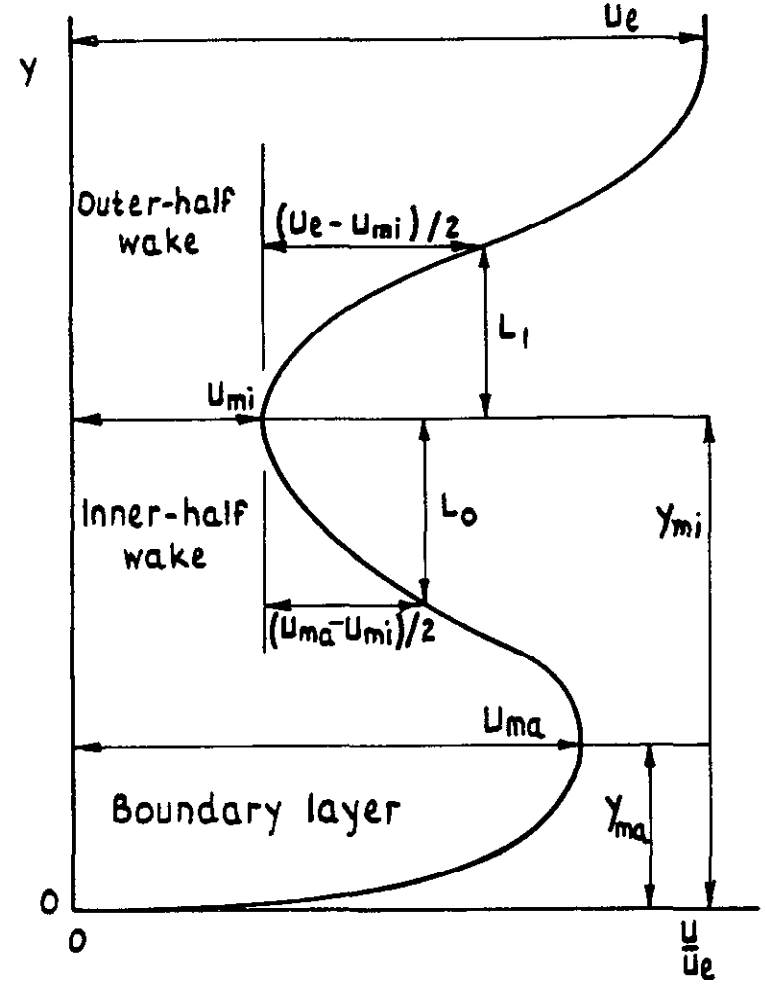

b Wake and boundary layer merged

Fig. 2 a & b Form of velocity profiles

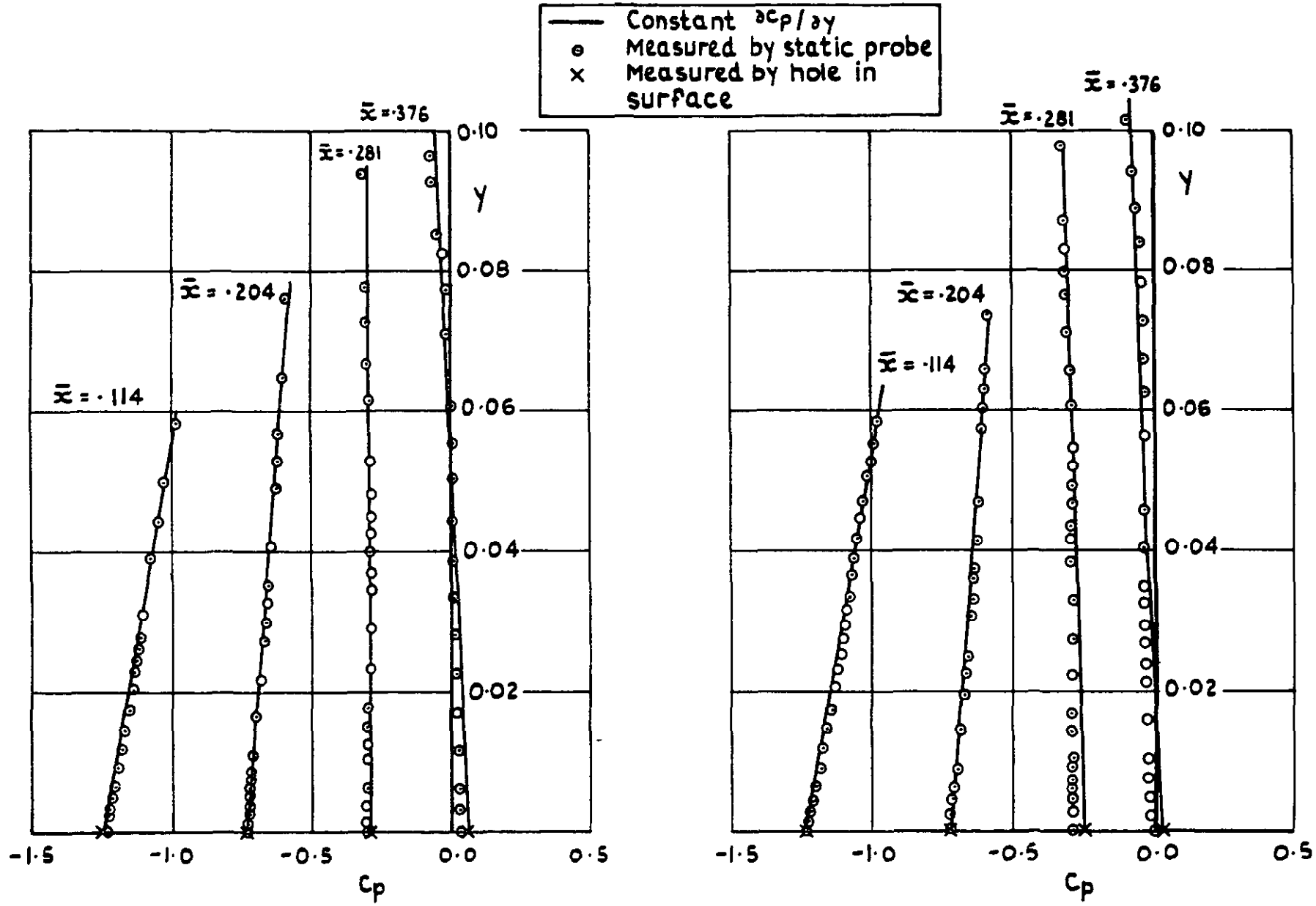

Flap deflection 30°, slot width 0·020c, $\alpha = 8°$

Flap deflection 30°, slot width 0·025c, $\alpha = 8°$

Fig. 3 Variation of static pressure normal to surface

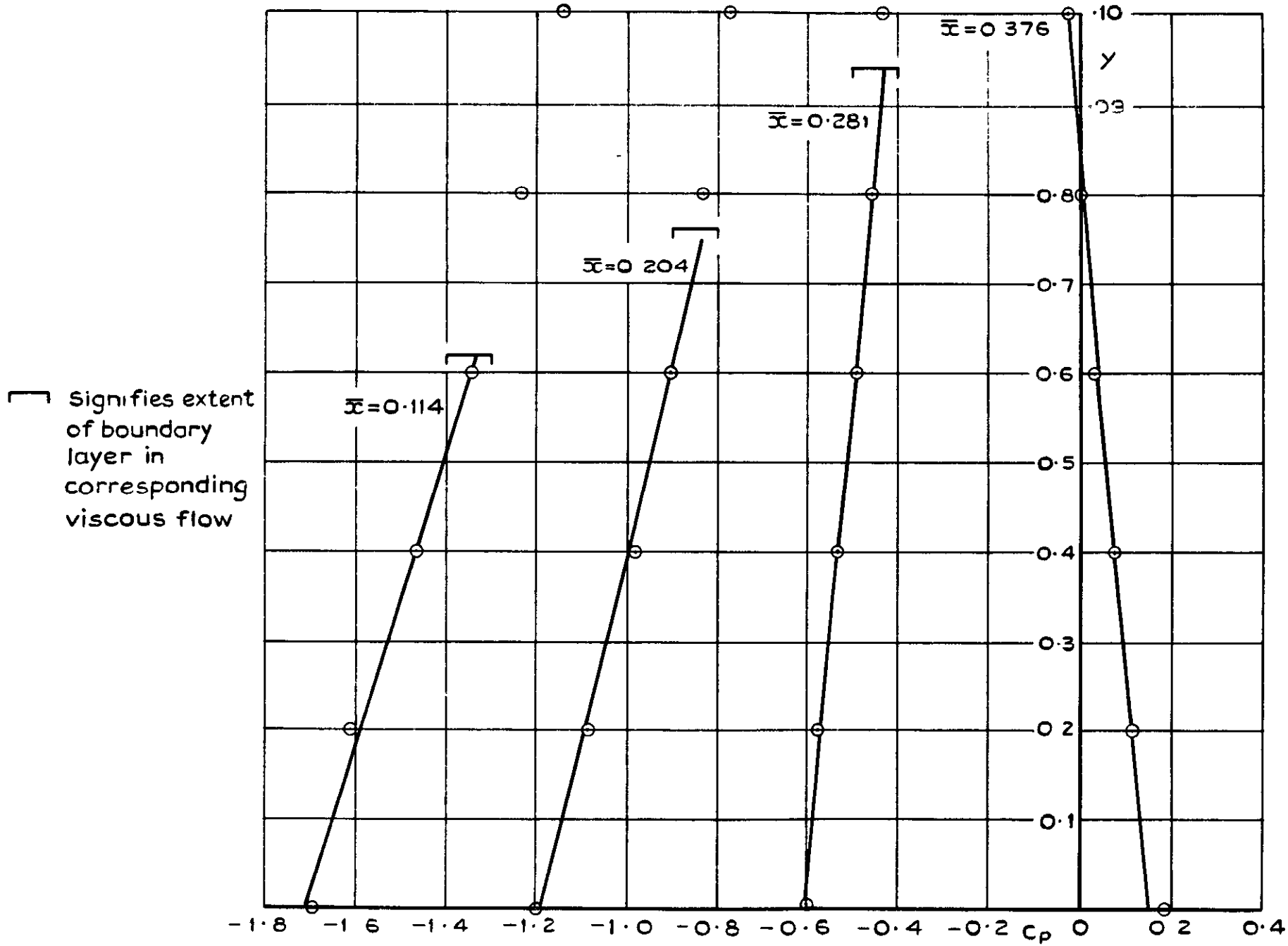

Fig. 4 Variation of static pressure normal to surface in inviscid flow

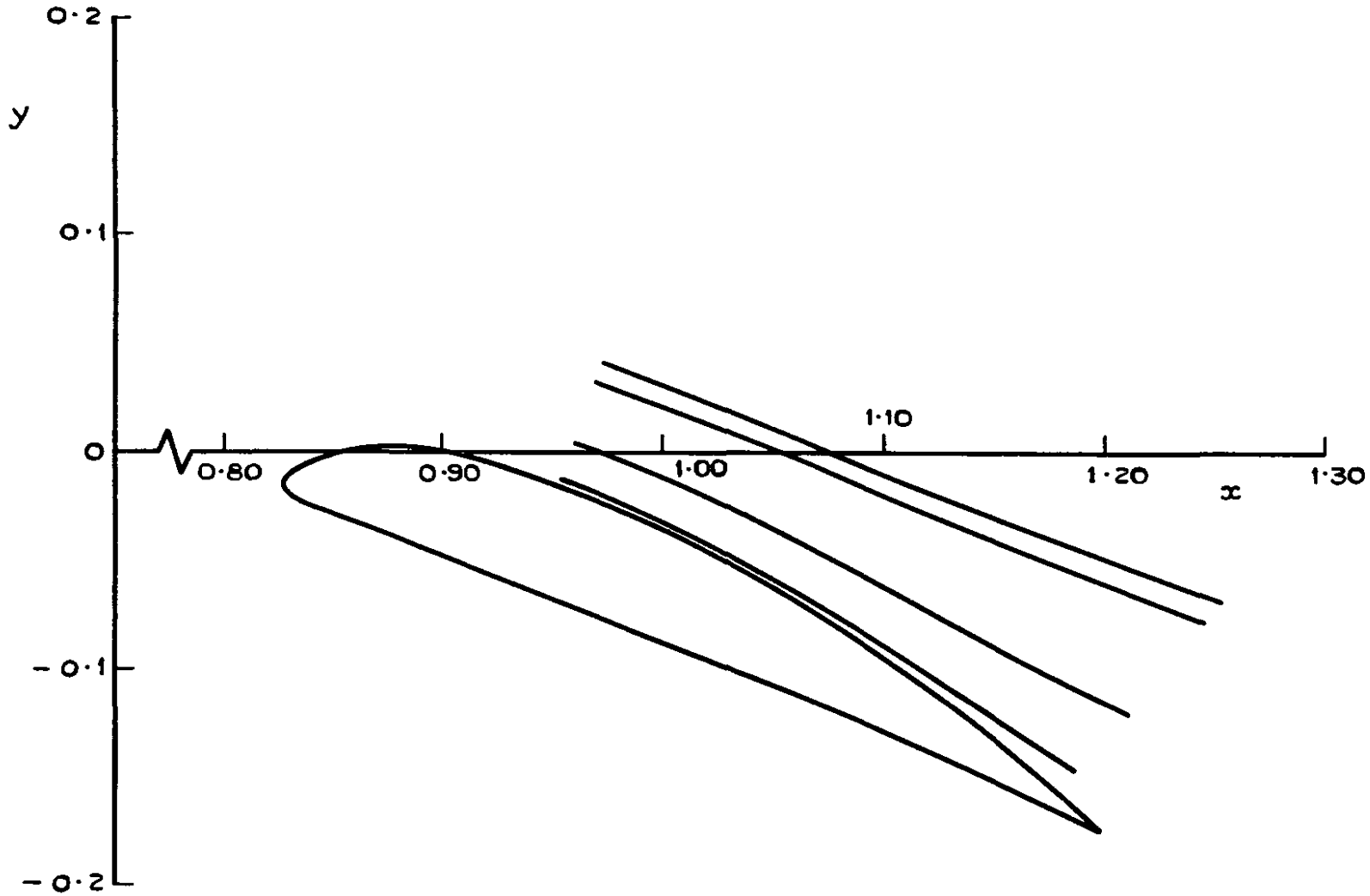

Fig.5 Shape of streamlines in flow above flap

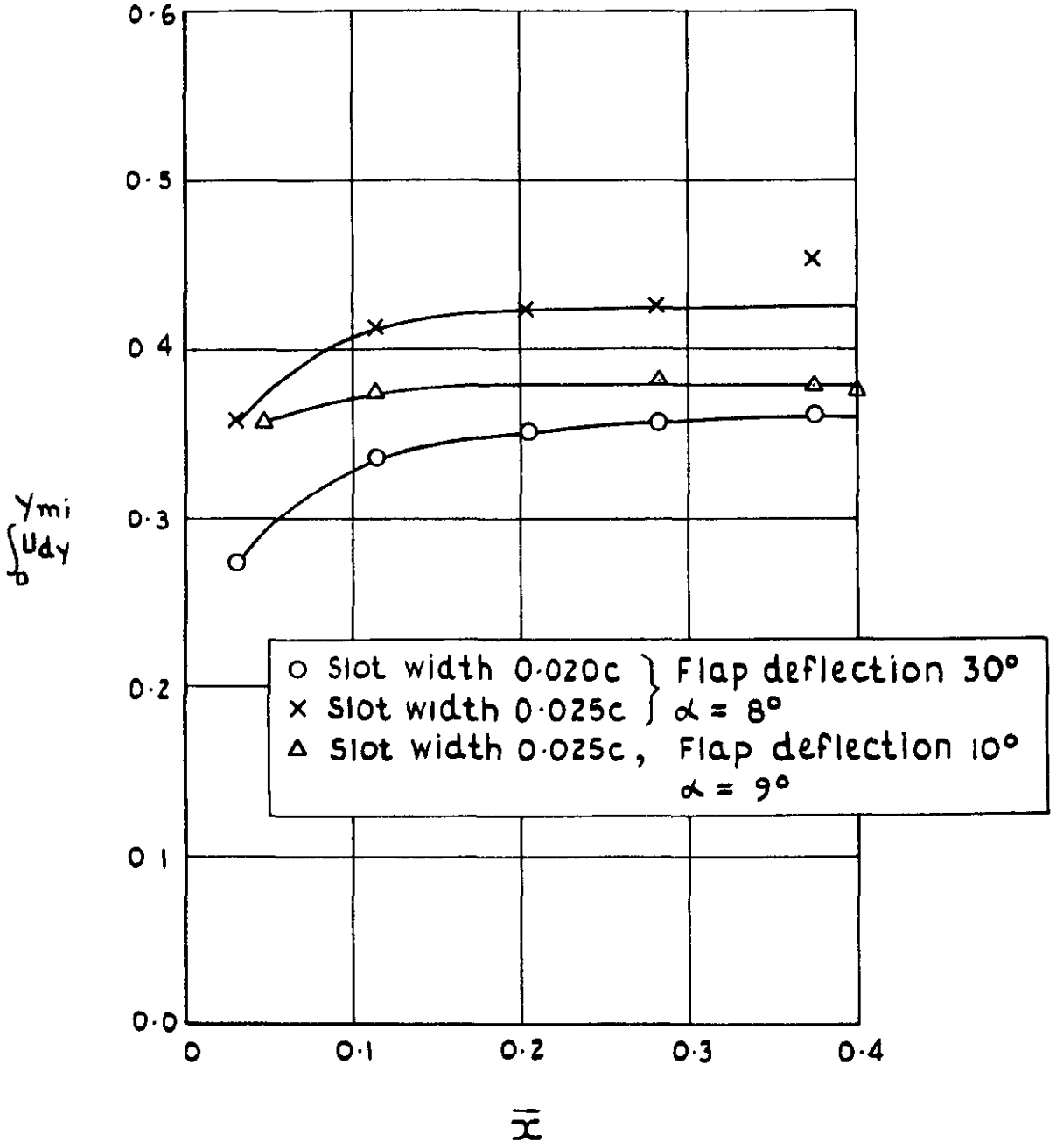

Fig.6 Measured mass flow in region below the velocity minimum

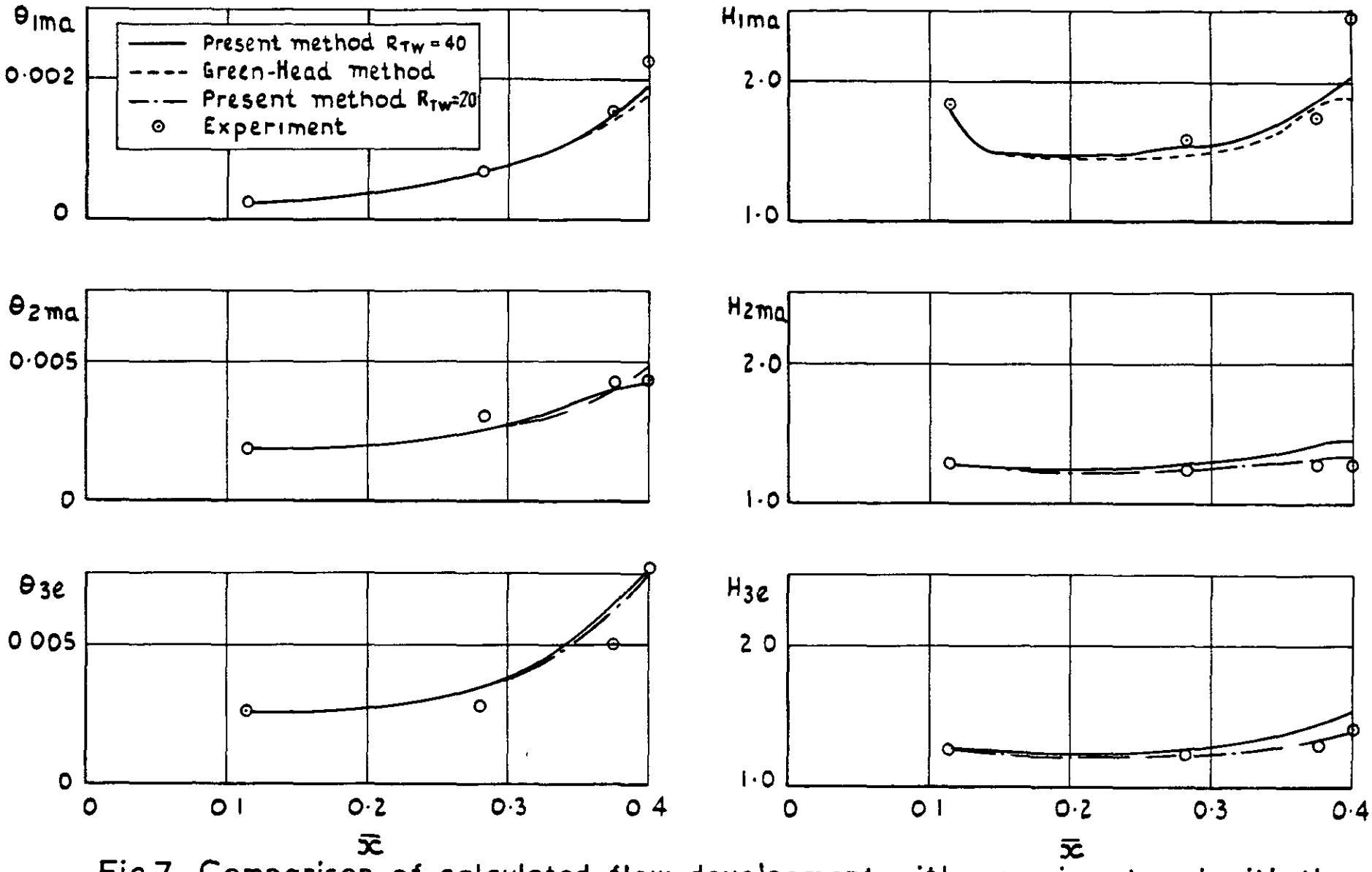

Fig.7 Comparison of calculated flow development with experiment and with the Green-Head method for a noninteracting case: flap deflection 10°, slot width 0·025c, $\alpha = 9°$, $\tau_{ma} = \tau_{mi} = F = 0$

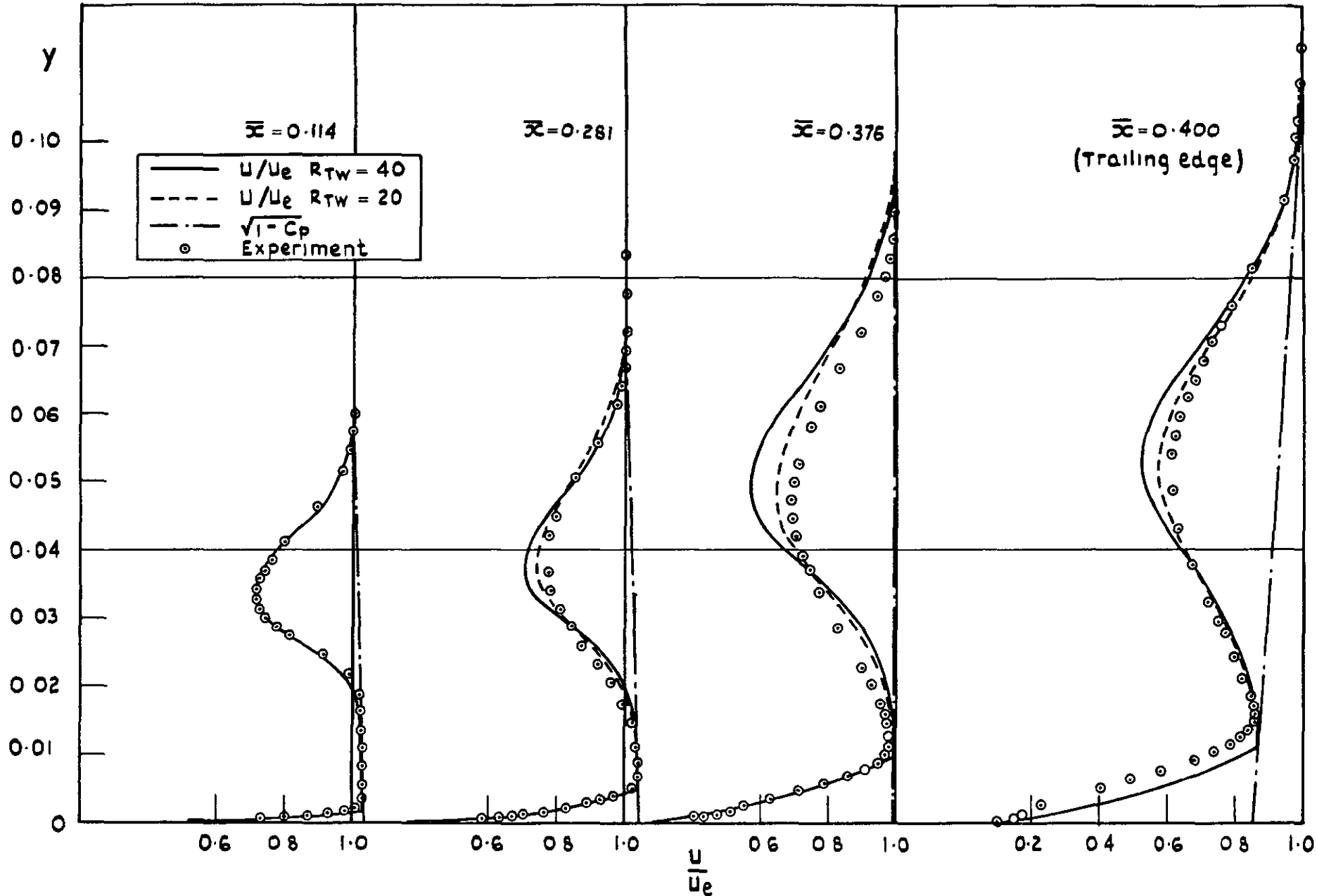

Fig. 8 Calculated velocity profiles compared with experiment: flap deflection 10°, slot width 0·025c, $\alpha = 9^{\circ}$, $\tau_{mi} = \tau_{ma} = F = 0$

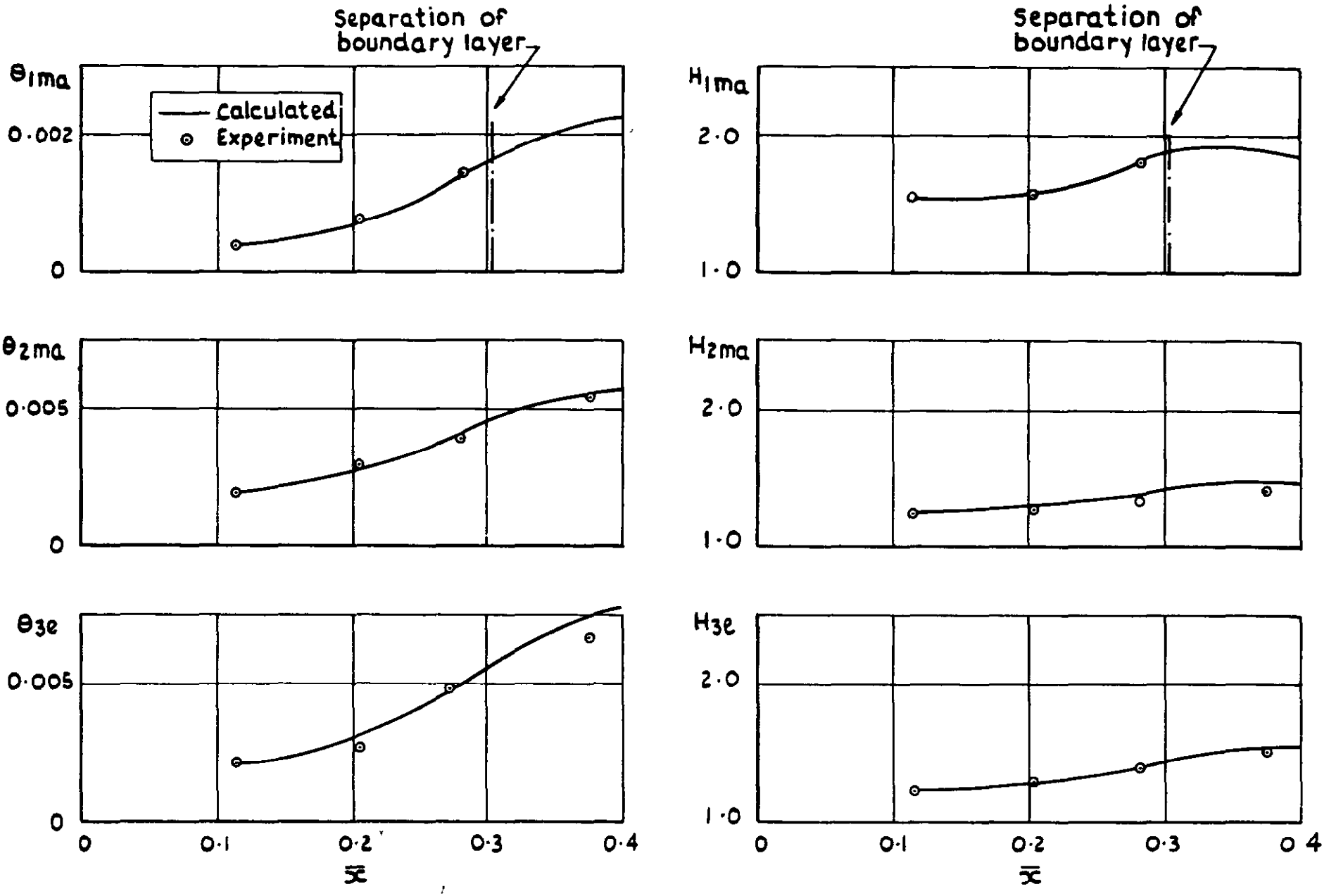

Fig.9 Comparison of calculated flow development with experiment: flap deflection 30°, slot height 0·025c, $\alpha = 8^{\circ}$, $\tau_{ma} = \tau_{mi} = F = 0$

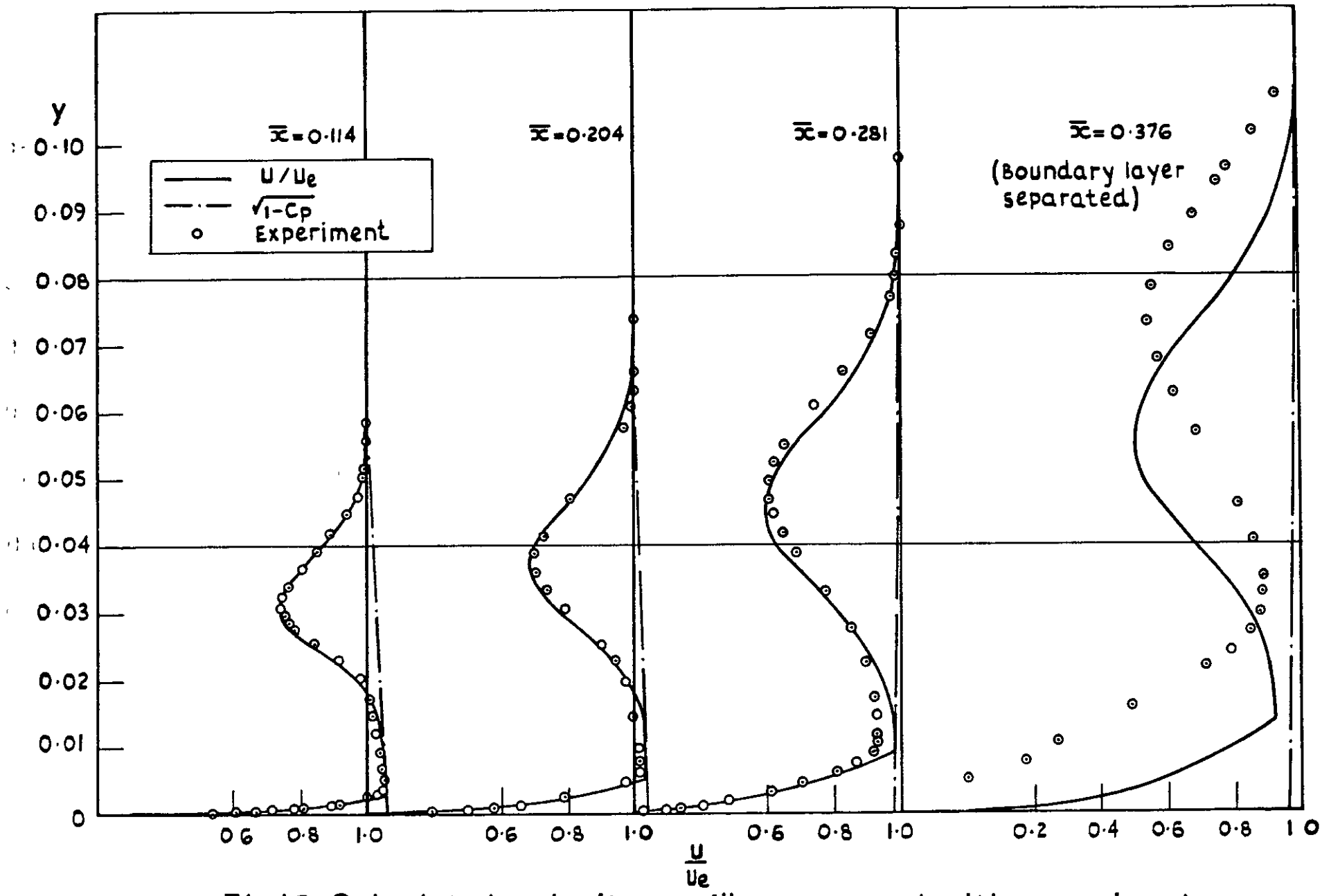

Fig.10 Calculated velocity profiles compared with experiment: flap deflection 30°, slot height 0·025c, $\alpha = 8°$, $\tau_{mi} = \tau_{ma} = F = 0$

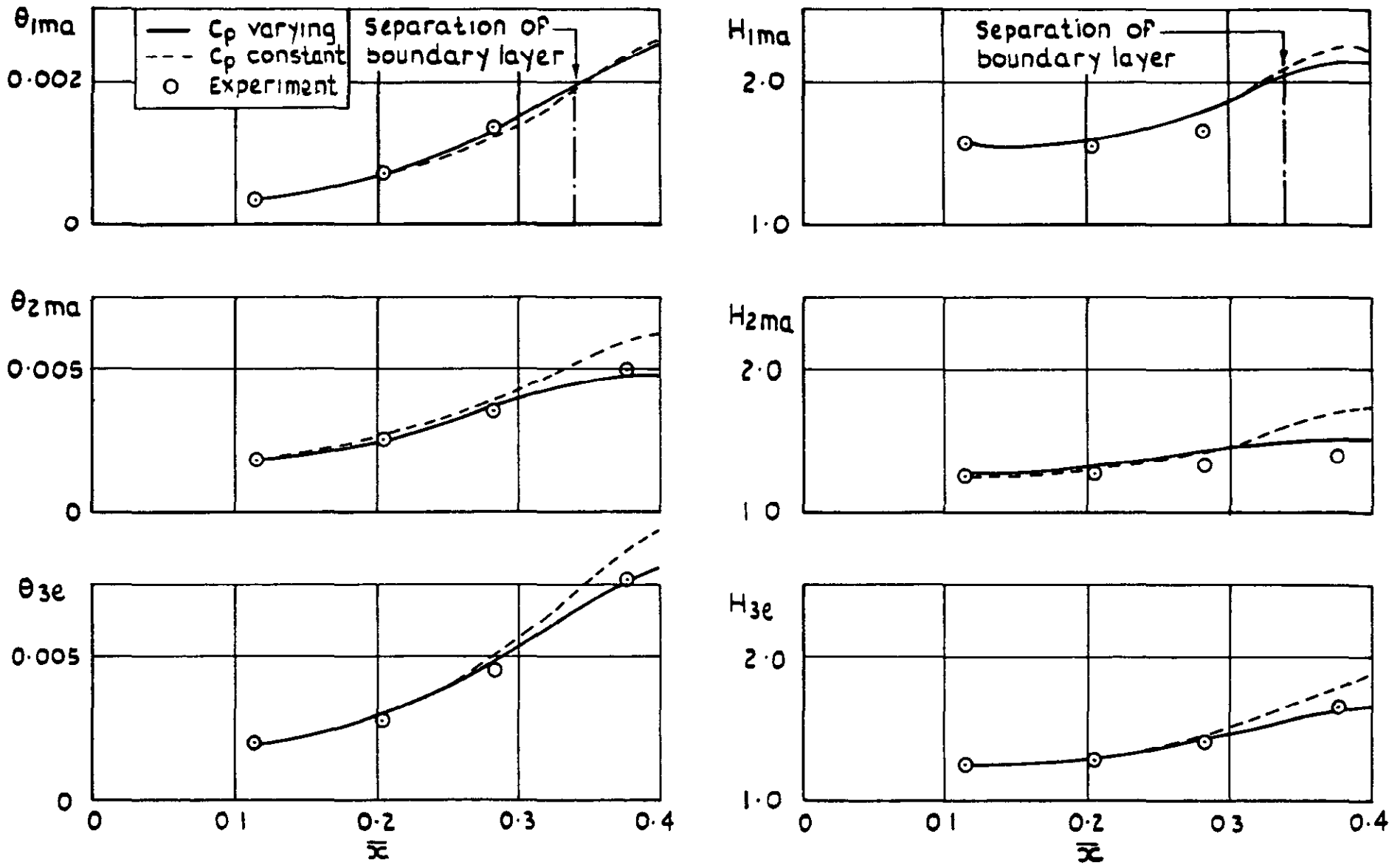

Fig.11 Comparison of calculated flow development with experiment and effect of pressure gradient normal to surface on calculations: flap deflection 30°, slot width 0·020c, $\alpha = 8°$, $F = \tau_{mi} = \tau_{ma} = 0$

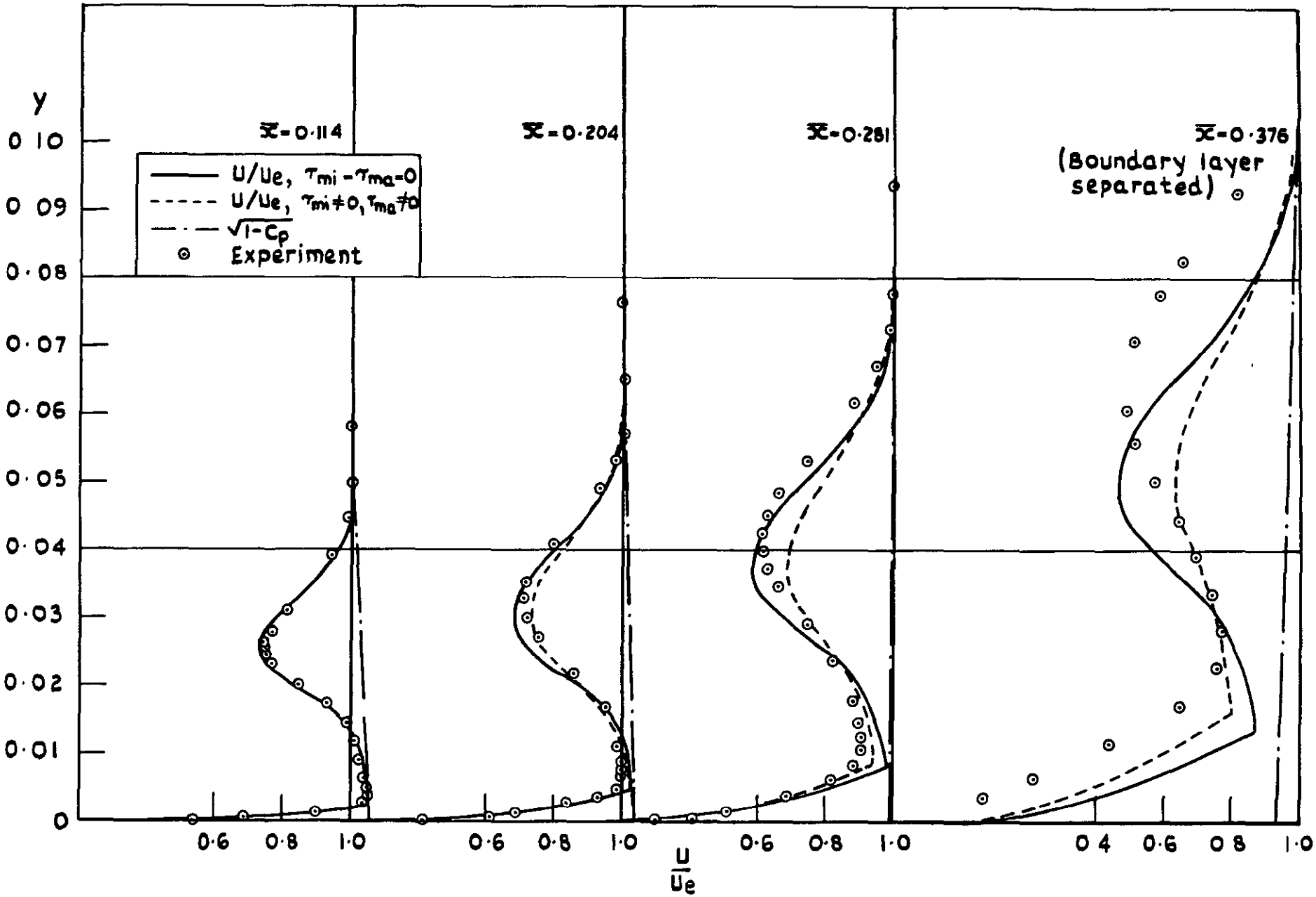

Fig 12 Calculated velocity profiles compared with experiment: flap deflection 30°, slot height 0·020c, $\alpha = 8^{\circ}$, F = 0

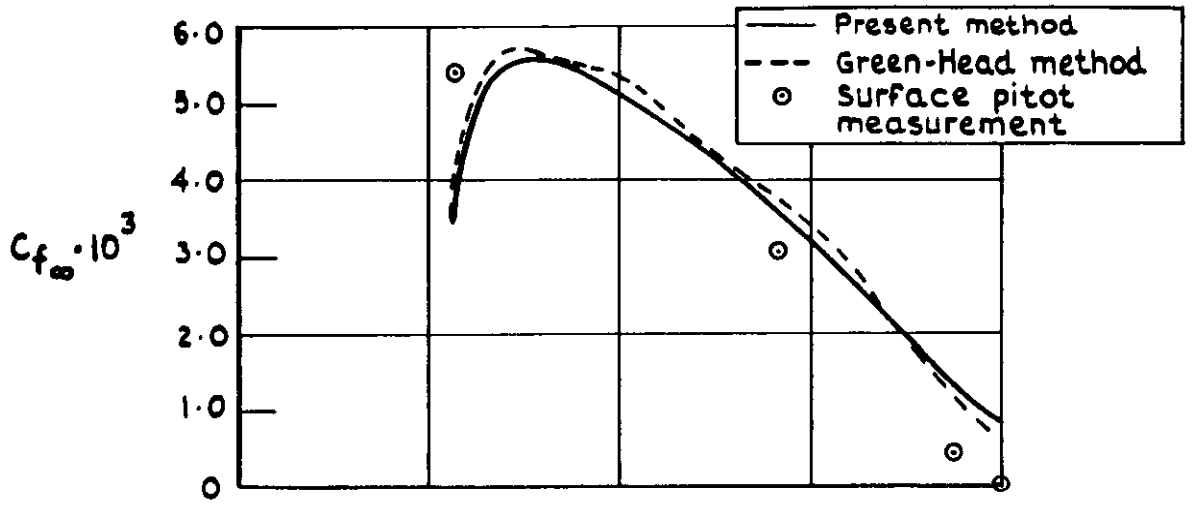

a Flap deflection 10°, slot width 0·025c, α = 9°

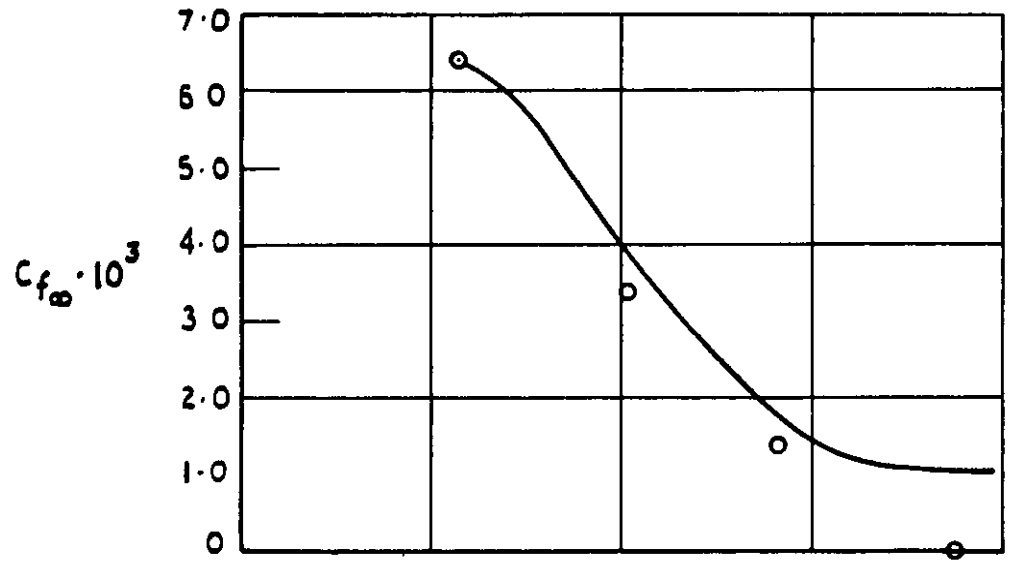

b Flap deflection 30°, slot width 0·025c, α = 8°

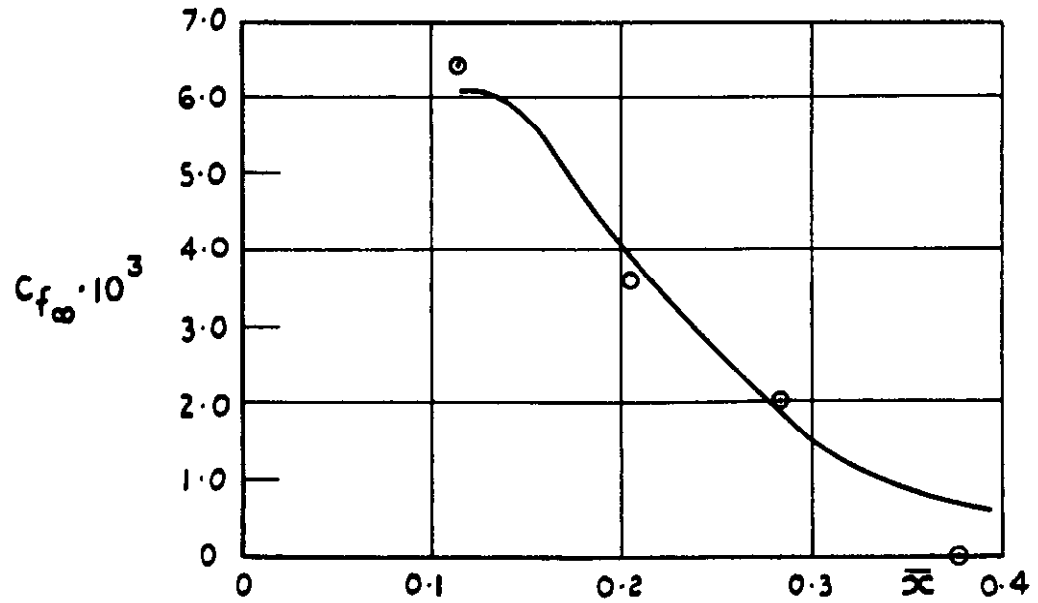

c Flap deflection 30°, slot width 0·020c, α = 8°

Fig.13 a–c Comparison of calculated skin friction with experiment

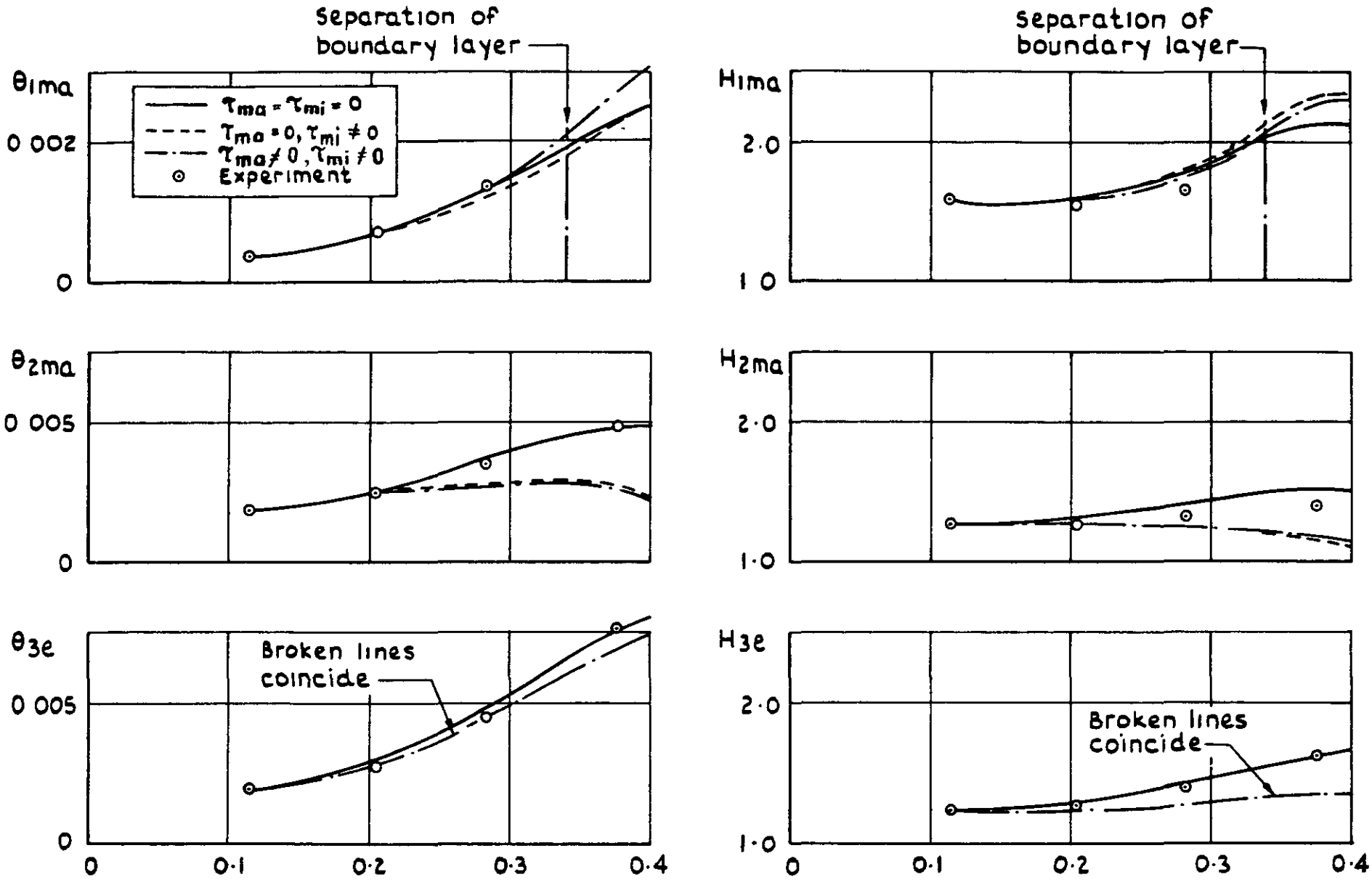

Fig.14 Effect of non zero τ_{ma} and τ_{mi} on calculations: flap deflection 30°, slot width 0·020c, α=8°, F = 0

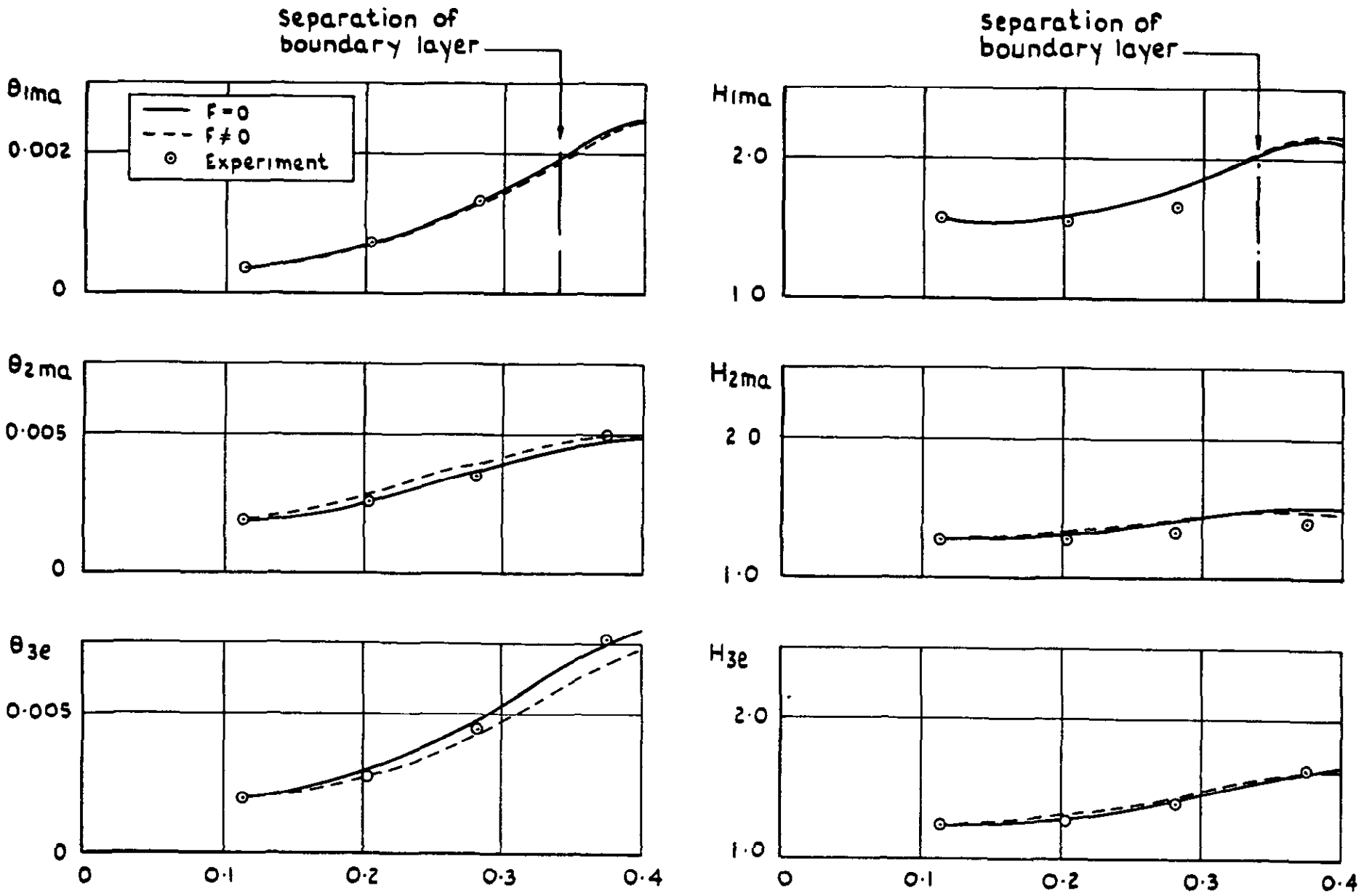

Fig.15 Effect of non zero value of F on calculations: flap deflection 30°, slot width 0·020c, $\alpha = 8°$, $\tau_{mi} = \tau_{ma} = 0$

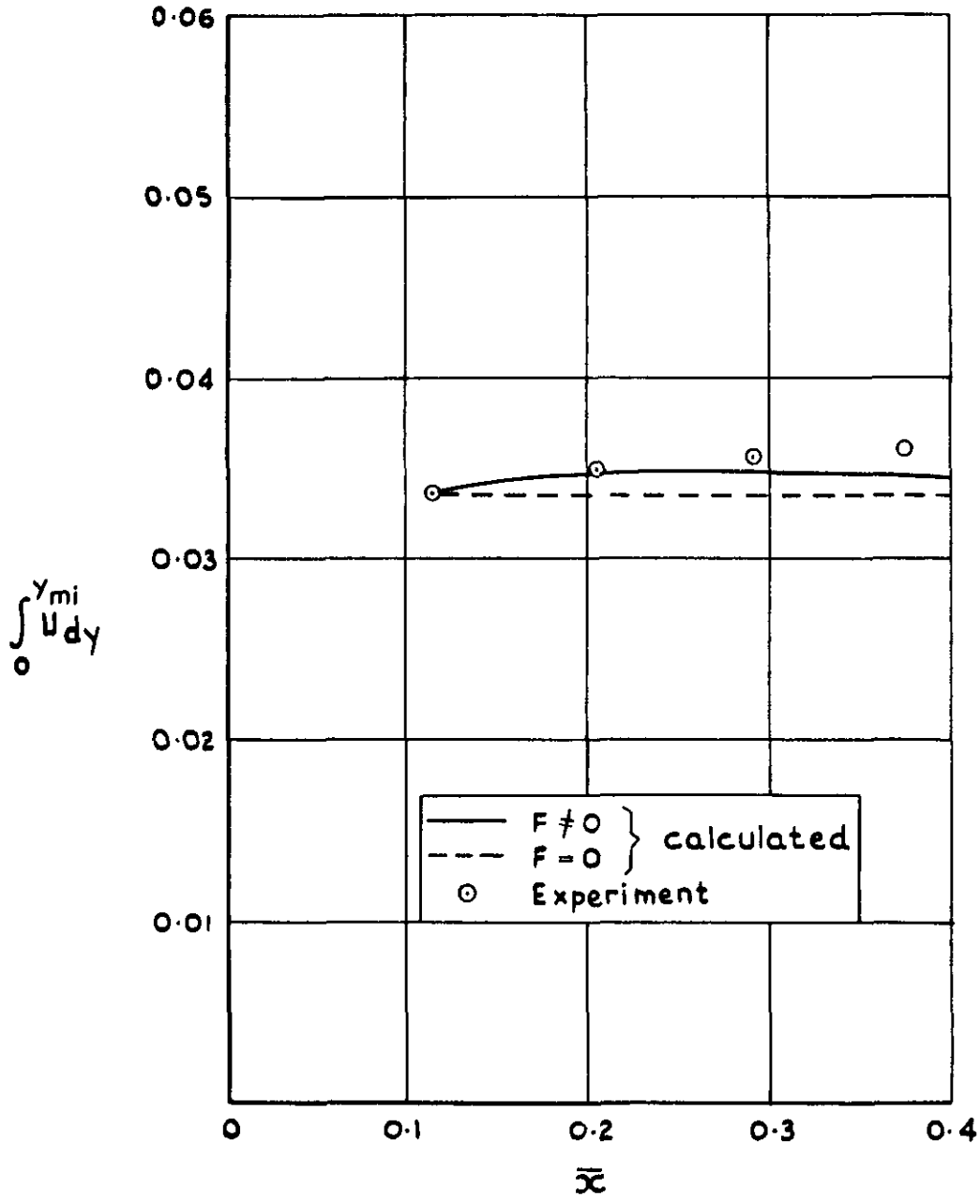

Fig.16 Comparison of calculated mass flow below velocity minimum with experiment: flap deflection 30°, slot width 0·020c, $\alpha = 8°$, $\tau_{ma} = \tau_{mi} = 0$

Current paper 1261

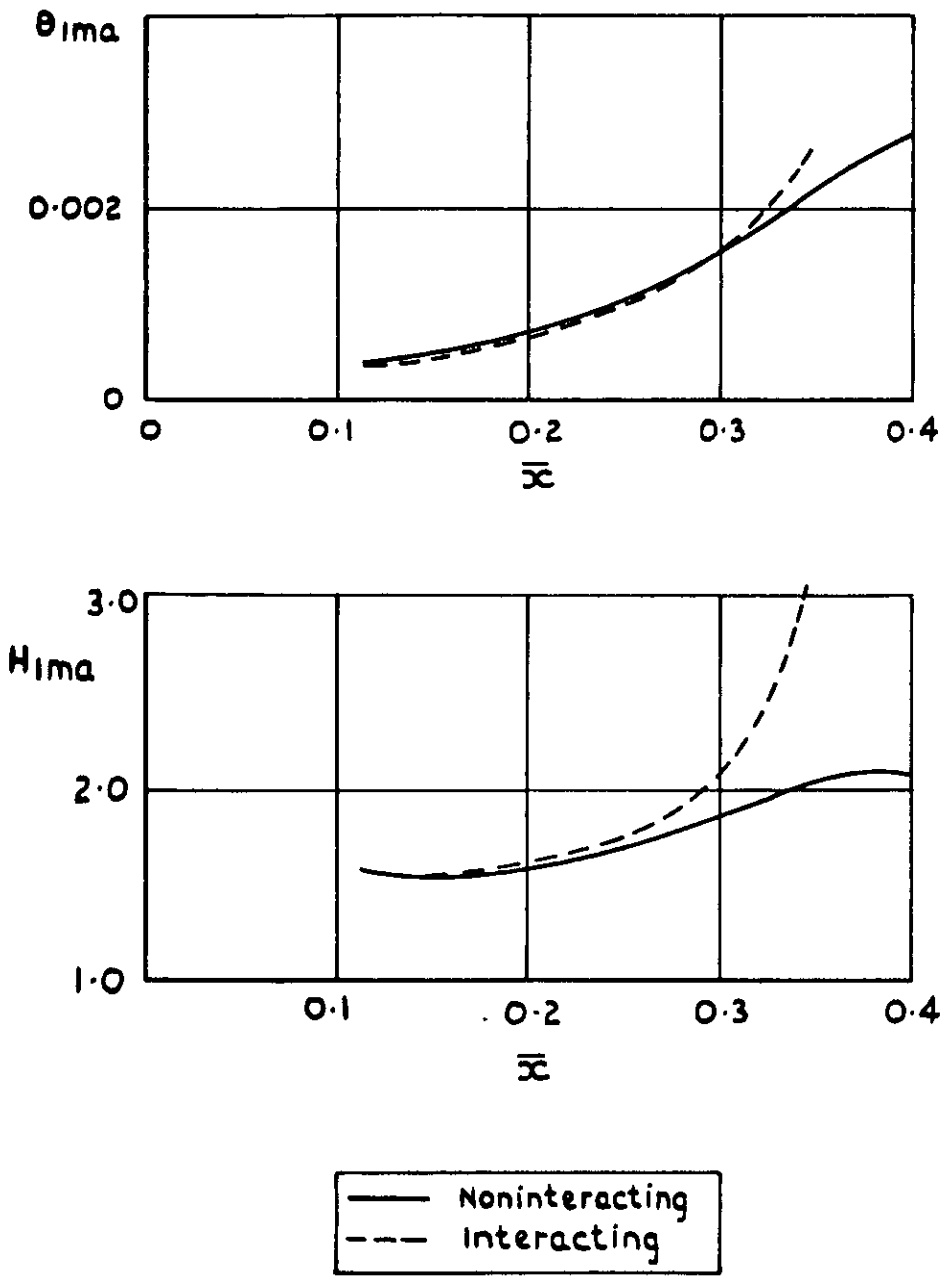

Fig. 17 Comparison of hypothetical interacting and noninteracting cases: $\tau_{ma} = \tau_{mi} = F = 0$

Printed in England for Her Majesty's Stationery Office by the Royal Aircraft Establishment, Farnborough Dd 505716 K4 10/73

ARC CP No.1267
June 1972

Irwin, H. P. A. H

A CALCULATION METHOD FOR THE TWODIMENSIONAL TURBULENT FLOW OVER A SLOTTED FLAP

532.517.4
533.6.011 1
533.694.22
532.526
533.6.048 3
532.526.7

An integral calculation method for the twodimensional turbulent flow over a slotted flap is described, taking into account the interaction of the wake from the main aerofoil with the boundary layer on the flap, and the variation of static pressure normal to the flap surface. The results are compared with experiment, and it is found that the method gives quite good agreement with the measured variation of the integral properties of the wake and boundary layer, and with the measured skin friction. The limitations of the method are discussed briefly in relation to the more complex approach of a differential method.

Cut here

ARC CP No.1267
June 1972

Irwin, H P. A. H.

A CALCULATION METHOD FOR THE TWODIMENSIONAL TURBULENT FLOW OVER A SLOTTED FLAP

532.517.4
533.6.011 1
533.694.22
532.526
533.6.048.3
532.526.7

An integral calculation method for the twodimensional turbulent flow over a slotted flap is described, taking into account the interaction of the wake from the main aerofoil with the boundary layer on the flap, and the variation of static pressure normal to the flap surface. The results are compared with experiment, and it is found that the method gives quite good agreement with the measured variation of the integral properties of the wake and boundary layer, and with the measured skin friction The limitations of the method are discussed briefly in relation to the more complex approach of a differential method.

ARC CP No.1267
June 1972

Irwin, H. P A H.

A CALCULATION METHOD FOR THE TWODIMENSIONAL TURBULENT FLOW OVER A SLOTTED FLAP

532.517.4
533.6.011 1
533.694.22
532.526
533.6 048.3
532.526.7

An integral calculation method for the twodimensional turbulent flow over a slotted flap is described, taking into account the interaction of the wake from the main aerofoil with the boundary layer on the flap, and the variation of static pressure normal to the flap surface. The results are compared with experiment, and it is found that the method gives quite good agreement with the measured variation of the integral properties of the wake and boundary layer, and with the measured skin friction. The limitations of the method are discussed briefly in relation to the more complex approach of a differential method.

Cut here

DETACHABLE ABSTRACT CARDS

DETACHABLE ABSTRACT CARDS

1974
Published by
HER MAJESTY'S STATIONERY OFFICE

To be purchased from
49 High Holborn, London WC1V 6HB
13a Castle Street, Edinburgh EH2 3AR
41 The Hayes, Cardiff CF1 1JW
Brazennose Street, Manchester M60 8AS
Southey House, Wine Street, Bristol BS1 2BQ
258 Broad Street, Birmingham B1 2HE
80 Chichester Street, Belfast BT1 4JY
or through booksellers

C.P. No. 1267

ISBN 011 470851 7